# Appendix D.2

# Redundancy Analysis of Prestressed Box Girder Superstructures under Vertical Loads

**By Jian Yang, Giorgio Anitori, Feng Miao and Michel Ghosn**

# Contents

# Redundancy Analysis of Prestressed Box Girder Superstructures under Vertical Loads

**by**

**Jian Yang, Feng Miao and Michel Ghosn**

## Abstract

This report describes the pushdown analysis of a typical prestressed concrete spread box girder superstructure when subjected to vertical loads simulating the effect of truck traffic. The prestressed concrete box girder bridge superstructure analyzed in the base case consists of two concrete box girders with a 120-ft simple span. The superstructure is loaded by HS-20 trucks and the loads are incremented until the bridge superstructure system fails. A sensitivity analysis is performed to study how variations in the bridge geometry, damage scenarios, member properties and bridge continuity affect the redundancy of the superstructure. Specifically, a Nonlinear Static Pushdown Analysis (NSPA) is used to investigate the sensitivity of the structure to variations in various parameters including: a) boundary conditions; b) damage of prestressing steel and damage scenarios; c) member capacity; d) dead load effect; e) span continuity. The behavior of the bridge superstructure is analyzed using the structural analysis software SAP2000. Load deformation curves are plotted for each variation in the bridge's properties and the ultimate load carrying capacities are compared to those of the basic bridge configuration.

Based on the results obtained thus far, it is observed that the redundancy ratios of simple span concrete box girder bridges are similar to those obtained for simple span steel box-girder bridges as described in the previous QPR. The number of bearing pads under a box has no effect on the redundancy ratios. The redundancy ratio $R_d$ for the damage scenario which assumes that the loss in the external web capacity is associated with the loss in the torsional resistance of the box is about 29% lower than the case when the loss in the external web does not affect the torsional capacity of the box. It is further observed that if 79% of the tendons in one box are damaged, the redundancy ratio falls below the $R_d$=0.5 that was proposed in NCHRP 406 as the redundancy criterion for damage scenario. It is also observed that the redundancy ratio for the ultimate limit state $R_u$ is not sensitive to changes in the member capacities or the dead load intensities for simple span bridges. However, the changes in member resistances will have some effect on the

redundancy ratios for the damaged limit state. The percent change in damage redundancy ratio $R_d$ may be on the order of about 60% of the percent change in member capacity.

For bridges which behave as simple spans for dead loads but are continuous for live load, we find that increasing the negative bending capacity can increase the redundancy ratios for both of the ultimate limit state and damaged scenarios while increasing the positive bending capacity decreases the redundancy ratio.

# 1. Introduction

The program SAP2000 is used in this Quarterly Report to perform the redundancy analysis of spread prestressed concrete box girder superstructures. In this report we use a grillage model where the webs of the boxes and the deck are modeled as equivalent beam elements following the approach proposed by Hambly (1991). Sensitivity analyses are conducted on the prestressed concrete box model and the results are compared to those of the composite steel box-girder bridges analyzed in the previous Quarterly Reports.

The analyses performed in this report are part of one row of the Matrix of bridge configurations that were set in the approved work plan. The list of parameters for box girder bridges that were scheduled for analysis is summarized in Table 1.1. The focus of the analysis is on the parameters that were found to be most important when we analyzed the redundancy ratios of steel box-girder bridges based on the assumption that these parameters have similar effect on concrete box-girder bridges. In fact, after comparing the results of the two types of bridges, it is observed that they have approximately similar redundancy ratios.

This report describes the structural modeling of concrete box-bridges, compares the results of the sensitivity analysis and provides a preliminary evaluation of the results.

Table 1.1 Summary of box-girder configurations and analyses that are to be addressed in this NCHRP12-86 project.

| **Loading scenario** | **Type of structure** | **Model** | **Spans** | **Design** | **Parametric analysis** | **Additional parameters** | **Damaged bridge scenario** |
|---|---|---|---|---|---|---|---|
| Vertical Load on Spread Boxes | • Steel open box<br>• P/s box | Fig. D | • Simple 150-ft<br>• Continuous 110-150-110 ft | • Two 6'x5'x4' boxes t=0.5 in. to 0.75 in.<br>• Same capacity P/s concrete boxes | • Bracing and diaphragms<br>• Resistance over dead load ratio | • Span length 200-ft<br>• Three steel boxes | • Fracture of one steel box at mid-span<br>• Reduce capacity of external web for concrete |

# 2. Prestressed Concrete Box Bridges

## 2.1 Base bridge model

The grillage mesh is generated following the guidelines presented by Hambly (1991) and Zokaie et al (1991). In a grillage analysis, the bridge system is discretized as longitudinal and transverse beam elements. For single cell, multi-cell and spread boxes, the longitudinal grillage beams are placed to coincide with the centerline of each web of the box girder and each beam represents the properties of its tributary area. For spread box girders each web represents half of the section properties of the prestressed concrete box girder.

The transverse beams consist of two types. The first type is used for the section falling outside the box girders. In this case, the transverse beam properties are based only on the slab thickness and corresponding material behavior. The second type of transverse beams is used to model the transverse properties of the box beam section considering the top plate of the box and the bottom plate of the box. The transverse beam properties are based on the transverse bending and torsion inertia of the box and are used to transfer the load between the longitudinal box beams.

The elastic properties required by the grillage analysis for each beam element include: (1) the modulus of elasticity, E; (2) the moment of inertia, I; (3) the shear modulus, G, and (4) the torsional constant, J. While the elastic bending properties are easy to calculate from basic strength of materials concepts, the torsional properties are most important for the analysis of box girder bridges and methods for their calculations are provided by Hambly (1991).

For the transverse beams representing the contribution of the slab alone with thickness t, the torsional constant is obtained as:

$$J = t^3/6 \quad \text{per unit length of slab} \tag{2.1}$$

As proposed by Hambly (1991), the value used for the torsion constant is only half $J = t^3/3$ that would be used for a thin rectangular section to account for the continuity between the slab elements.

The torsional constant of the beams modeling the transverse properties of the box is given as:

$$J = 2h^2 \frac{t_1 \times t_2}{t_1 + t_2} \quad \textit{per unit width of cell} \tag{2.2}$$

Where $t_1$ and $t_2$ are the thicknesses of the top and bottom flange and h is the height of the section.

The distortion of concrete box is ignored on the assumption that the concrete box is sufficiently thick which along with the presence of diaphragms will reduce the effect of distortion. Accordingly, the torsional constant of the box section is determined using the torsional constant of a closed section with the equation given by Hambly (1991).

$$J = \frac{4\,A_o^2}{\sum \frac{s_i}{t_t}} \tag{2.3}$$

Where $S_i$ and $t_i$ are respectively the length and thickness of each segment of the closed box as shown in Fig. 2.1, $A_o$ is the area of the box enclosed within the center-line of the webs and flanges.

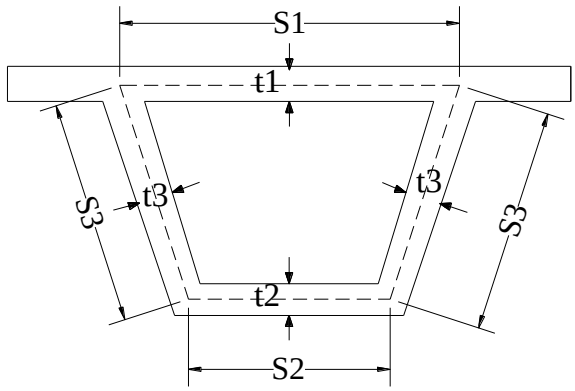


**Figure 2.1 Geometrical Parameters corresponding to torsional constant of a box girder**

The simply-supported span bridge with the precast prestressed concrete box section shown in Figure 2.2 is considered for the base case. Longitudinal elements represent the longitudinal bending behavior of the prestressed concrete box. Two types of transverse elements are adopted as mentioned above, the first one (point-line in Figure 2.2) represents the slab between the two boxes, the second type (dashed-line in Figure 2.2) represents the transverse bending and torsional properties of the box beams (Hambly 1991). The nonlinear behavior at high loads is represented for the longitudinal and transverse beam elements by moment-rotation relationships assuming a lumped plasticity model.

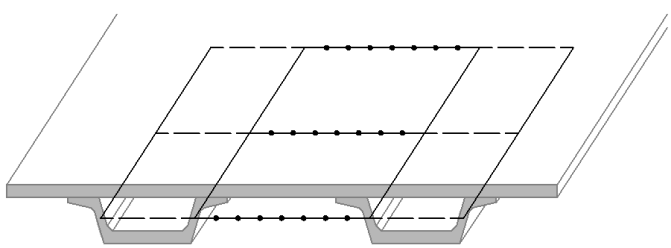

**Figure 2.2 Grillage model for box girder bridge.**

**Table 2.1 Concrete material properties**

| Parameters | Concrete of box | Concrete of slab |
|---|---|---|
| 28 Day Strength (ksi) | 7.250 | 4.350 |
| Tension Strength (ksi) | 0.6400 | 0.4900 |
| Crushing Strain | 4.000E-3 | 4.000E-3 |
| Tension Strain Capacity | 0.1319E-3 | 0.1304E-3 |
| Elastic Modulus (ksi) | 4853 | 3759 |

Realistic stress-strain curves are adopted to represent the material behavior and calculate the moment-curvature relationships. In particular, Mander's model (Mander, 1984) was adopted for the concrete with the parameters listed in Table 2.1. Figure 2.3 gives a plot of the stress-strain relation for the boxes' concrete and that of the deck.

The stress-strain curve for the bare prestressing strand shown in Figure 2.3 (c) has been determined by a Ramberg-Osgood function to give a smooth transition between the elastic and plastic behavior. Collins and Mitchell (1991) give the following expressing for low-relaxation strands with:

$$f_{pu} = 270 \text{ ksi (1860 MPa)}$$

$$f_{ps} = E_p \varepsilon_{ps} \left\{ 0.025 + \frac{0.975}{\left[1 + (118\varepsilon_{ps})^{10}\right]^{0.10}} \right\} \leq f_{pu} \tag{2.4}$$

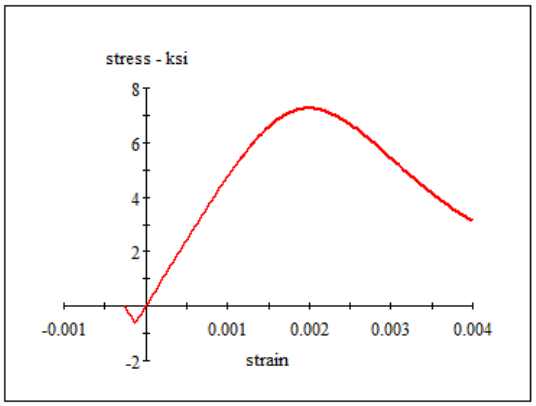


(a) Concrete of box 7.25 ksi (50 Mpa)

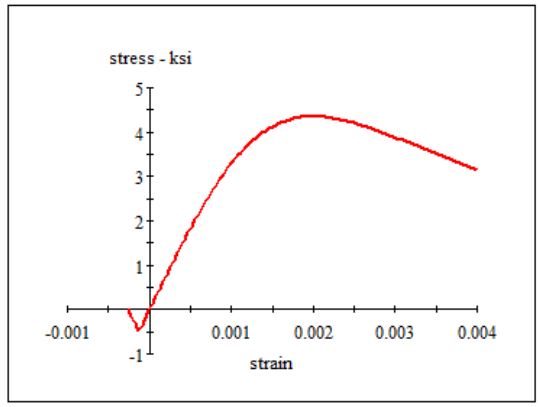


(b) Concrete of slab 4.35 ksi (30 Mpa)

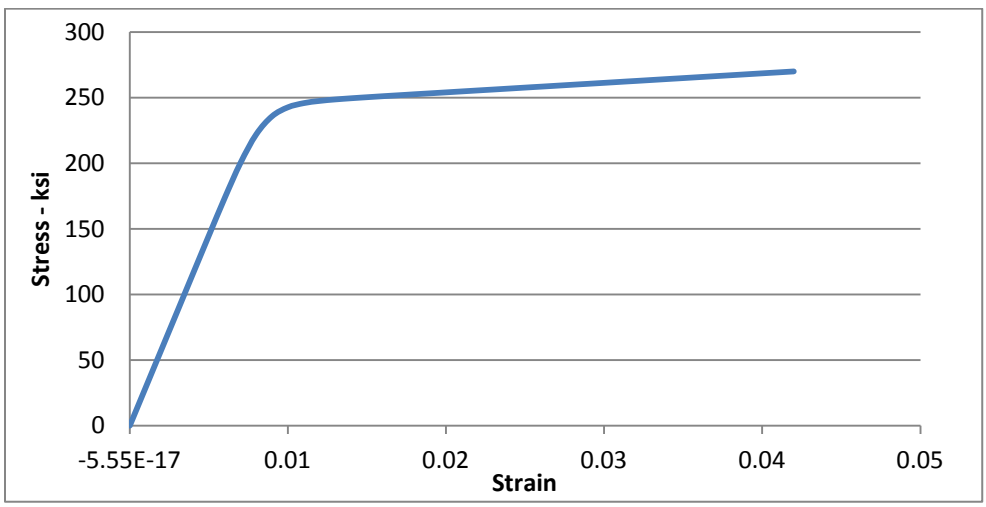


(c) 270 ksi (1860 MPa) low-relaxation prestressing steel

**Figure 2.3 Stress strain relationships of bridge materials**

In this study, uncoupling between the torsional and bending properties is assumed and the linear torsion properties remain in effect throughout the loading process. The nonlinear bending behavior is modeled using a moment versus plastic rotation curve for each beam element.

The moment versus plastic rotation curve of a box-girder member is obtained by first calculating the moment versus curvature relationship using strength of material principles. A plastic hinge length, $L_p$, is assumed to be ½ of the depth of the cross-

section as done during the analysis of steel I-girder and box girder superstructures. When the element length is short, the plastic hinge length on both sides of the element should not exceed the total length of the element therefore $L_p$ should be less than ½ of the beam element length. Otherwise, ½ the element length is used for the plastic hinge length.

The bridge configuration that is analyzed for the base case consists of twin prestressed concrete box girders carrying a simple span 120-ft long bridge. The dimensions of the boxes are shown in Figure 2.4.

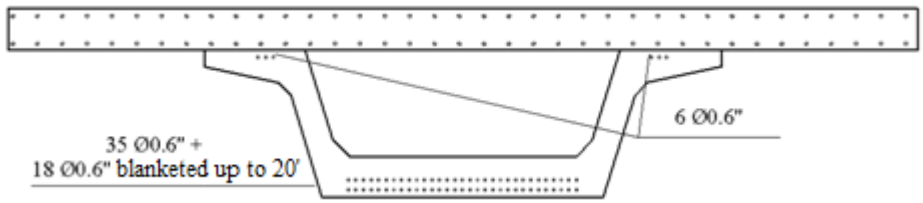


(a) Configuration of prestressing steel

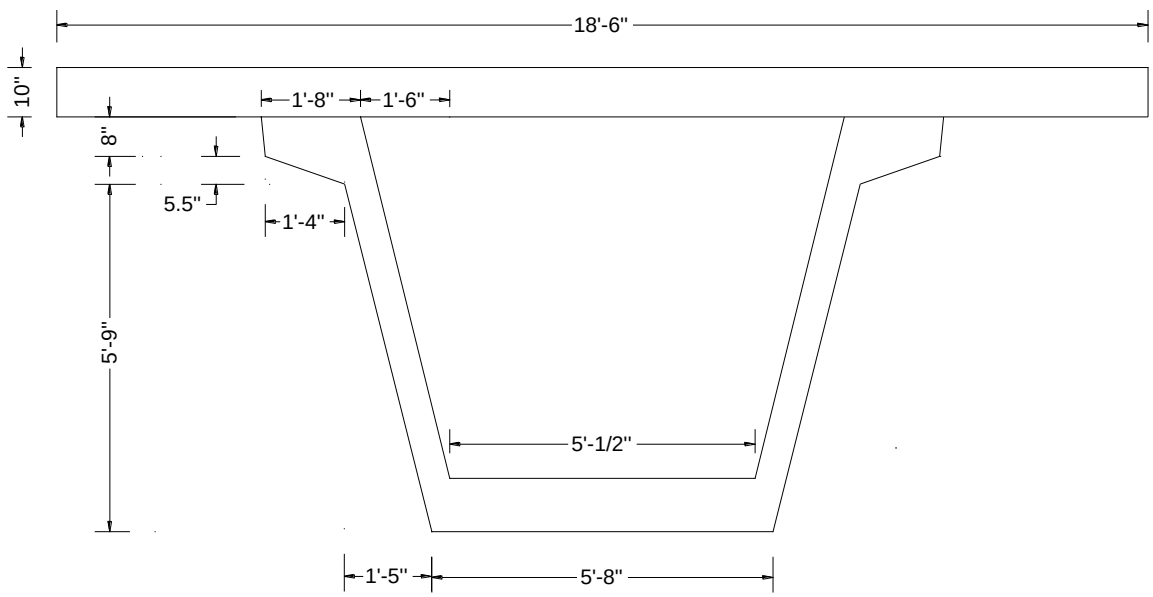


(b) Dimensions of one box

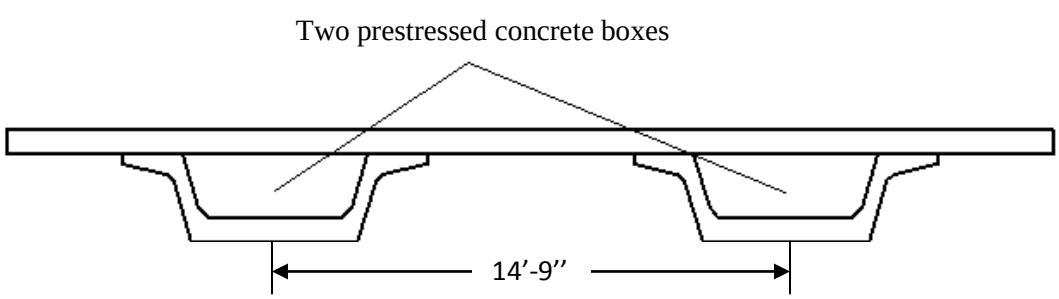


(c) Spacing of two boxes

**Figure 2.4 Detailed dimensions of cross-section of the twin box bridge**

The dead load consists of the weight of the concrete boxes and the concrete deck and barriers. The dead load is calculated directly by the program SAP 2000 according to section area and density of material. The weight of the concrete deck applied on each of the two interior boxes is W1=0.0027 kip/in, the weight of the concrete deck and barriers applied on each of the two exterior beams is W2=0.0427 kip/in.

The composite moments of inertia and torsional constants for each of the beams are listed in Table 2.2 for the grillage model of Figure 2.8. All the longitudinal beams are assumed to have the same properties. The end transverse beams are assumed to have half the values of the properties of the middle transverse beams.

**Table 2.2 Elastic properties of bridge model**

| | Moment of Inertia I ($in^4$) | Torsional Constant J ($in^4$) |
|---|---|---|
| Longitudinal beams | 2,326,011 | 2,246,346 |
| Transverse box beams | 2,738,861 | 1,970,058 |
| Transverse slab beams | 2,787 | 12,006 |

Moment-curvature relationships for positive moment for one box are obtained using the program Xtract. Because the initial curvature of the beam before applying any load is negative and because SAP2000 cannot accommodate negative curvatures, the vertical axis of the moment curvature is shifted up and a negative moment of a magnitude equal to the shift is applied on the beam. Because the end 20-ft of 18 strands (out of the 35 total strands) are blanketed, the adjustment in the M-phi curves is different at the end of the beam from the adjustment at 20-ft from the end. Therefore, a negative moment $M_1$ is applied at the end of the beam while $M_2$ is applied at 20-ft from the end as shown in Figure 2.8.b. Because one longitudinal beam represents half a box in the model, the moments for each longitudinal beam are taken as one half of the moments obtained from the program Xtract. The moment-curvature relationships for each composite box are shown in Figure 2.5 for the cross section with blanketed tendons and the section where all 35 strands contribute to the section capacity. The corresponding moment-curvatures for the one beam are plotted in Figure 2.6 which also shows the vertical adjustments to the origins values $M_1$ and $M_2$. The moment-curvatures for the transverse beams representing

the contribution of the slab to the lateral distribution of the load is shown in Figure 2.7. In this example, we assume that the beam representing the transverse contribution of the box remains in the linear elastic range.

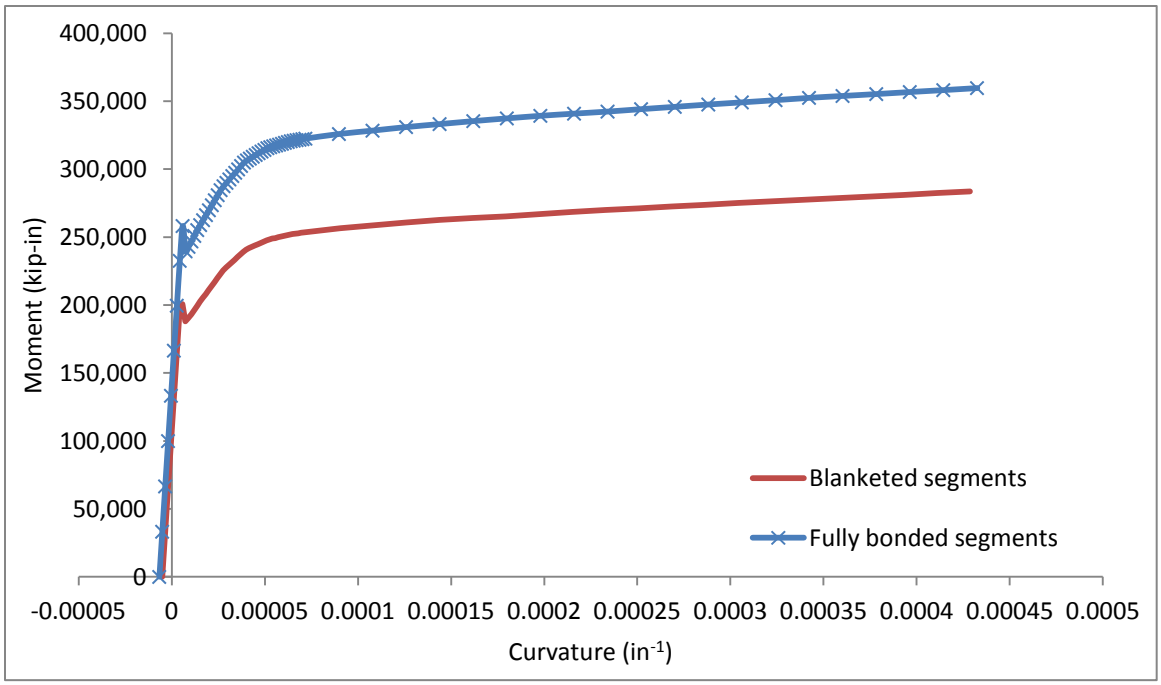


**Figure 2.5 Moment curvature curves of one prestressed concrete box from Xtract program**

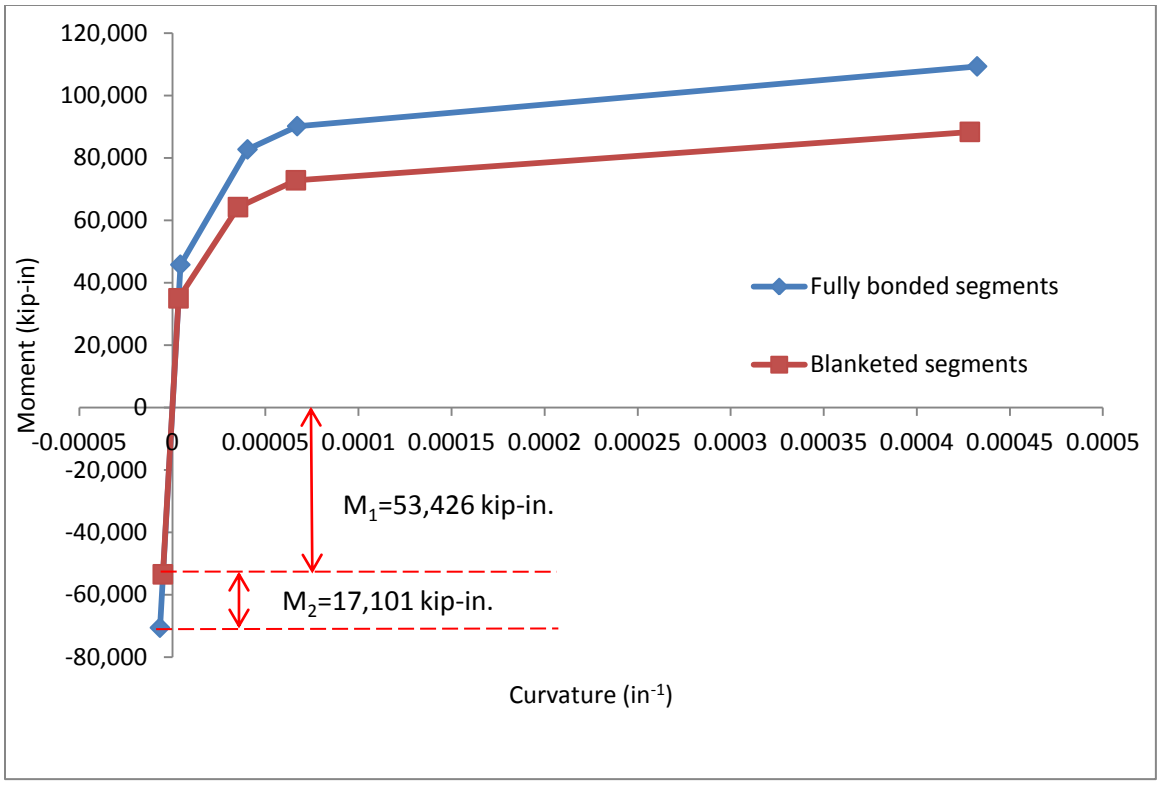


**Figure 2.6 Shifted moment curvature curves of longitudinal beam (half box) accounting for the prestressing moments**

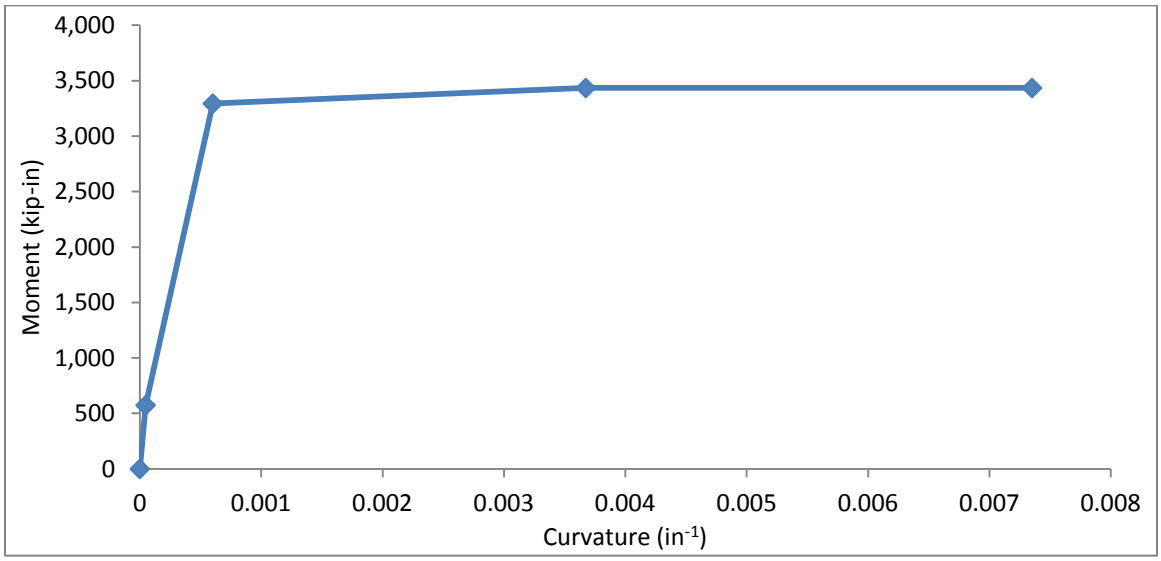


**Figure 2.7 Moment curvature curve of transverse slab beams in SAP2000 model**

Failure of the superstructure is defined in terms of the load that leads to having one longitudinal concrete girder reach its ultimate moment capacity which is defined as the point at which the concrete crushes or prestressing steel ruptures. Alternatively, ultimate failure can also take place when a plastic mechanism forms which is associated with numerical instabilities in the SAP2000 analysis algorithm which occur when several members are in their plastic range even though none of them has crushed yet. While the slab model accounts for the nonlinear material behavior, crushing in one slab element is not considered to define bridge failure although a mechanism would. This approach is adopted because the simplistic model of the slab used in this analysis does not very accurately account for the interaction between the two directions of the slab whose behavior resembles that of a two-way plate rather than the assumed grid system. Therefore, the main focus of the analysis is the global failure of the system represented by the failure of the main longitudinal members rather than local failures in the slab or other secondary components. As demonstrated in previous Quarterly Reports, the model used provides an accurate modeling of the global behavior of the system and properly represents the distribution of the load to the longitudinal members.

In addition to the dead load, the bridge is loaded by one HS-20 truck positioned longitudinally in the center of the middle span and laterally such that the edge wheel is applied over the external web. The SAP2000 model and HS-20 truck load positions are shown in Figure 2.8 (a).

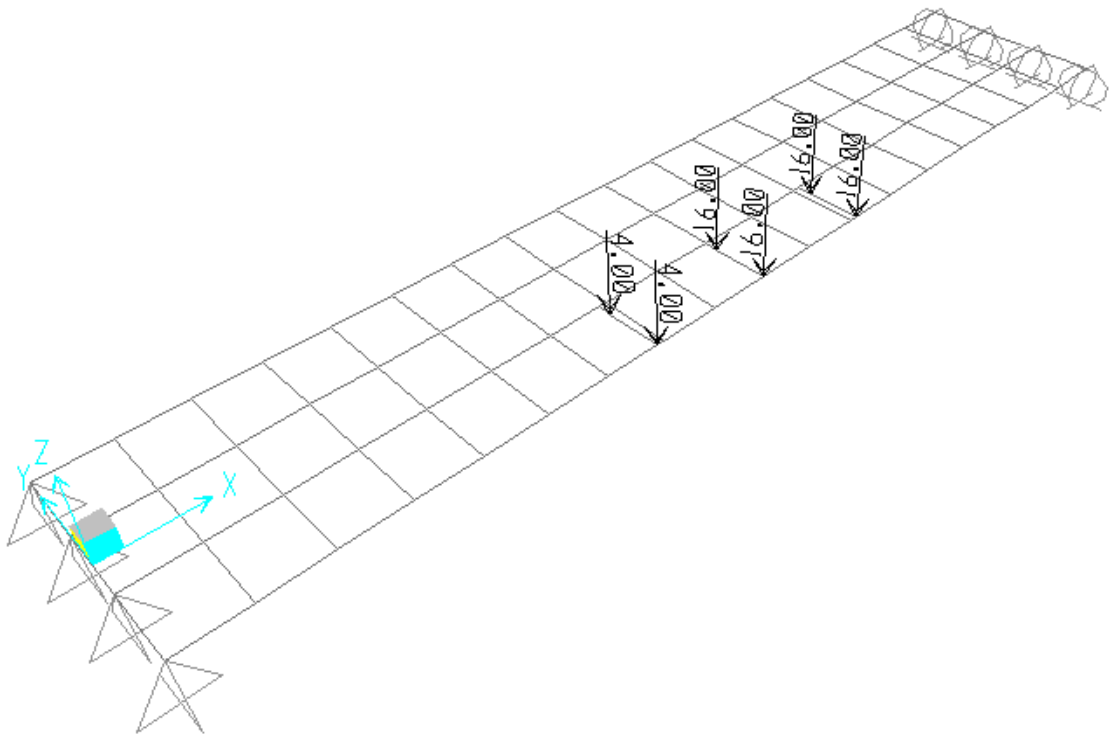


(a) 3-D SAP2000 model and configuration of HS-20 truck

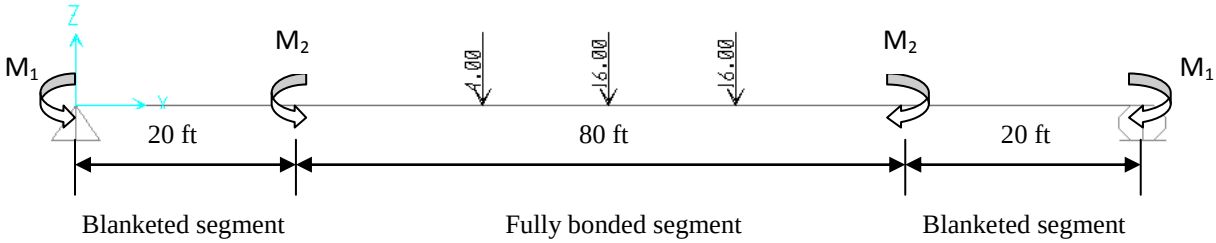


(b) Configuration of initial negative moments to account for shift in M-phi curves due to prestressing

**Figure 2.8 SAP2000 model of the 120 ft simple span bridge (Unit: kip, ft)**

## 2.2 Pushdown analysis of basic bridge model

From the moment-curvature relationship shown in Figure 2.5, the longitudinal beam (one half of the composite steel box girder) section is found to have an ultimate positive moment capacity equal to $R=M^{+}= 179,577$ kip-in.

Using the results of a linear elastic analysis, the moment due to the dead load at the mid-span of a girder (considering the initial negative moments $M_1$ and $M_2$ applied to account for the shift in the moment-curvature relationship) is obtained as DL= 53,081 kip-in. The external girder will carry a linear elastic moment equal to 7,008 kip-in due to one AASHTO HS-20 vehicle. If a traditional linear elastic analysis is used to evaluate the load carrying capacity of the bridge, the number of HS-20 trucks that would lead to failure would be obtained from:

$$LF_1 = \frac{R - DL}{DF_1 LL_{HS-20}} \tag{2.5}$$

Where R is the member's unfactored moment capacity, DL is the member's unfactored dead load, $DF_1$ is the linear elastic distribution factor, and $LL_{HS-20}$ is the total live load moment effect due to the HS-20 vehicle. For improved accuracy, the product $DF_1$ $LL_{HS-20}$ is obtained from the linear elastic results as the highest live load moment effect for any longitudinal member from the SAP2000 results rather than using the AASHTO load distribution factors.

Using Eq. (2.5) is consistent with traditional methods for evaluating the load carrying capacity of the bridge superstructure. In fact, $LF_1$ in Eq. (2.5) is similar to the Rating Factor R.F. used to assess the load rating of existing bridges. The difference between R.F. and $LF_1$ is that Eq. (2.5) ignores the load and resistance factors and considers only the static load. The load and resistance factors are not needed in this analysis because we are interested in evaluating as accurately as possible the load carrying capacity of the bridge superstructure rather than providing safe envelopes for design and load rating purposes.

In this analysis, we express the load carrying capacity of the superstructure in terms of multiples of the HS-20 load that the bridge can safely carry.

For this particular bridge, with R=179,577 kip-in, DL= 53,081 kip-in and $DF_1$ $LL_{HS-20}$ =7,008 kip-in, the application of Eq. (2.5) indicates that the load factor that leads to first member failure in positive bending assuming traditional linear elastic analysis methods is $LF_1$=18.05. This result indicates that if one is to follow traditional bridge analysis methods, the first member of the bridge will reach its ultimate capacity at a load equal to 18.05 times the effect of one HS-20 truck.

The next step of the analysis process consists of performing the nonlinear pushdown analysis for the superstructure. The push down analysis is performed for the originally intact structure and for a damaged structure. The damage scenario selected for the Base case consists of removing the entire external web of one box which may model the effect of major damage due to overall deterioration or as consequence of an impact with the box. Two damage alternatives are investigated for the damage scenario. In Case 1, we assume the torsional constant (J=2,246,346 $in^4$) of the adjacent web is not affected by the damaged of the external web, while in Case 2 the torsional constant of the remaining half box is calculated as an open section with J= 18,278 $in^4$. Case 1 represents a 50% reduction in the box capacity concentrated near the edge web which could simulate corrosion type damage. Case 2 represents accidental shearing type damage to half the box. Figure 2.9 gives the total reactions versus the maximum vertical deflection of the bridge when a nonlinear incremental load analysis is performed. The results of the pushdown analysis are summarized in Table 2.3.

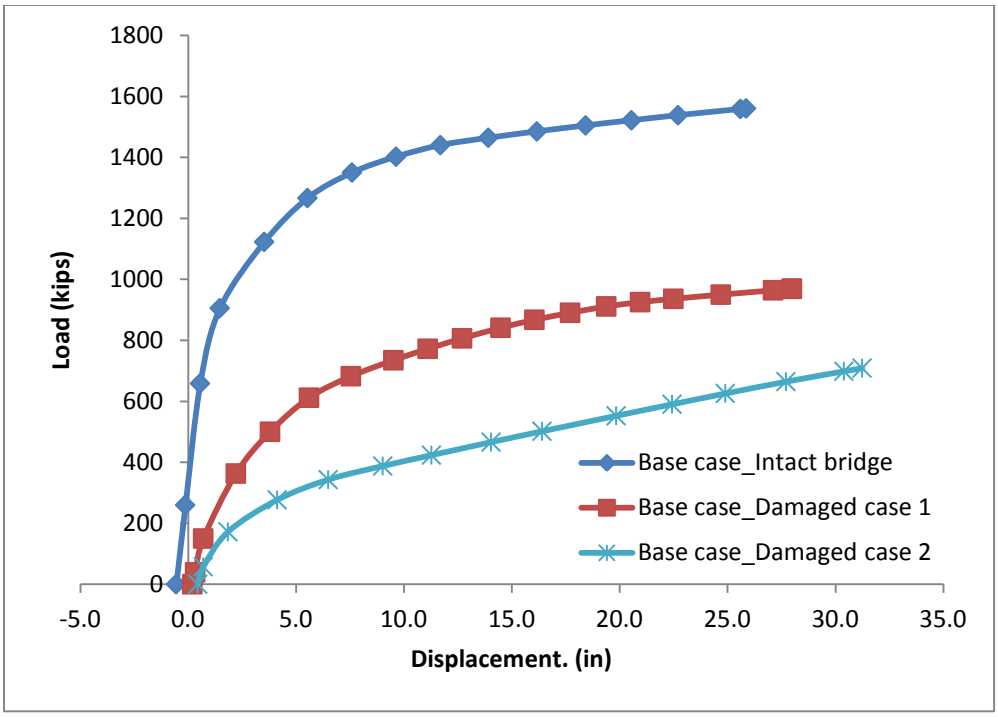


**Figure 2.9 Load deflection relationship of 120-ft simple span prestressing concrete bridge**

**Table 2.3 Results of the pushdown analysis of the prestressed concrete box bridge**

| Load factors | $LF_1$ | $LF_{300}$ | $LF_{200}$ | $LF_{100}$ | $LF_u$ | $LF_d$ ① | $LF_d$ ② |
|---|---|---|---|---|---|---|---|
| SAP2000 | 18.05 | 16.87 | 18.53 | 20.40 | 21.68 | 13.46 | 9.85 |

Note: ① represent damage case 1; ②represent damage case 2.

Figure 2.9 shows that the ultimate capacity of the superstructure is 1,013.6 kips when the HS-20 vehicle is incremented by a factor, $LF_u$ equals to 1,560.9 kips/72 kips=21.68, as shown in Table 2.3. A displacement equal to span length/300 (4.8 in) is reached when the load factor, $LF_{300}$ is equal to 1,214.4 kips/72 kips=16.87. A displacement equal to span length/200 (7.2 in) is reached when the loads are incremented by a factor, $LF_{200}$= 1,334.5 kips/72 kips=18.53. A displacement equal to span length/100 (14.4 in) is reached when the load factor reaches a value, $LF_{100}$ equal to 1,469.0 kips /72 kips =20.40.

To analyze the capacity of the bridge assuming that the external beam has been totally damaged due to an unexpected event such as an impact from a passing truck or corrosion

of prestressing steel, the analysis of the superstructure is performed after completely removing the exterior longitudinal beam but keeping the truck load in the same position. The two damage scenario alternatives consist of the cases where the torsional constant is reduced so that the remaining web keeps the same constant of the undamaged case. In Case 2, we assume that the box loses its torsional stiffness and we assume that the remaining torsional stiffness is due to an open section. The nonlinear pushdown analysis is executed after the damaged external longitudinal composite girder is removed from the mesh but the live load over the external longitudinal beam is transferred to the remaining undamaged girders through the transverse beam elements.

The analysis of the damaged bridge reveals that the ultimate capacities of the damaged bridge case 1 and case 2 are reached when the HS-20 vehicle is incremented by a factor $LF_d$ equal to 969.2 kips /72 kips =13.46 and 709.0 kips /72 kips =9.85, as shown in Table 2.3.

## 2.3 Evaluation of bridge redundancy

According to NCHRP 406 redundancy is defined as the capability of a structure to continue to carry loads after the failure of the most critical member. For a structure that has not been previously subjected to a damaging event, the capacity of the superstructure to resist the first failure of a member using traditional analysis methods is represented by $LF_1$. Also, the ability of the "original undamaged superstructure", herein referred to as "intact superstructure", to continue to carry load even after one member reaches its nominal capacity, is represented by the load factors $LF_u$. However, if a superstructure may become nonfunctional due to large displacements its capacity may be represented by $LF_{300}$, $LF_{200}$ or $LF_{100}$. In NCHRP 406, the functionality criterion was set in term of $LF_{100}$ which is the load factor at which a displacement equal to span length/100 is reached. For this reason the functionality criterion is set as $LF_f$=$LF_{100}$.

Recently, some researchers have defined robustness as the capability of the system to carry some load after the brittle failure of a main load carrying member (see for example,

Faber et al, 2008). According to NCHRP 406, the evaluation of system robustness is equivalent to evaluating the redundancy for the damaged system which is represented by the load factor $LF_d$.

If we accept the definition of redundancy as the capability of a structure to continue to carry loads after the failure of the most critical member, then comparing the load multipliers $LF_u$, $LF_f$, $LF_d$ to $LF_1$would provide non-subjective and quantifiable measures of system redundancy and robustness. Based on that logic, NCHRP 406 defines three deterministic measures of redundancy referred to as redundancy ratios or system reserve ratios which relate the system's capacity to the most critical member's "assumed" capacity:

$$R_u = \frac{LF_U}{LF_1}$$

$$R_f = \frac{LF_f}{LF_1} \qquad (2.6)$$

$$R_d = \frac{LF_d}{LF_1}$$

where $R_u$ =redundancy ratio for the ultimate limit state, $R_f$=redundancy ratio for the functionality limit state, $R_d$= redundancy ratio for the damage condition.

The redundancy ratios as defined in NCHRP 406 provide nominal deterministic measures of bridge redundancy (and robustness). For example, when the ratio $R_u$ is equal to 1.0 ($LF_u$=$LF_1$), the ultimate capacity of the system is equal to the capacity of the bridge to resist failure of its most critical member. Based on the definitions provided above, such a bridge is nonredundant. As $R_u$ increases, the level of bridge redundancy increases. A redundant bridge should also be able to function without leading to high levels of deformations as its members plasticize. Thus, $R_f$ provides another measure of redundancy. Similarly, a redundant bridge structure should be able to carry some load after the brittle fracture of one of its members, and $R_d$ would provide a quantifiable non-

subjective measure of structural redundancy for the damaged bridge which has also been defined as robustness.

The NCHRP 406 criteria for bridge redundancy require that: a) the ratio of the ultimate system capacity to first member failure, $R_u$, should be equal or exceed 1.3; b) the ratio of the system capacity to resist a maximum vertical deflection of span length/100, defined as $R_f$, should be equal to or exceed 1.10 times the capacity of the bridge to resist first member failure; and d) that a damaged system should have a system capacity equal to or exceeding 0.50 times the capacity of the intact system to resist first member failure ($R_d \geq 0.5$).

The criteria of NCHRP 406 were selected following the redundancy and reliability analysis of many bridge superstructures of different material, section type, span length, number of beams, and beam spacing. In keeping with traditional practice that classified bridges with four parallel I-girders as redundant, reliability and redundancy criteria were selected in NCHRP 406 so that they are met on the average by typical four-I-girder bridges. Possible adjustments to these criteria will be considered in this NCHRP 12-86 Project, if necessary, based on the additional results that this project will produce and in consultation with the Project Panel.

For the bridge superstructure system analyzed above, the redundancy ratios are obtained as:

$R_u=LF_u/LF_1=21.68/18.05=1.20<1.30$

$R_f=LF_f/LF_1= 20.40/18.05=1.13>1.10$

$R_d^{①}=LF_d/LF_1= 13.46/18.05=0.74>0.50$

$R_d^{②}=LF_d/LF_1 = 9.85/18.05=0.54>0.50$

These redundancy ratios are listed in Table 2.4.a. It is noted that these values are very close to those obtained for simple span steel box-girder bridges as described in the previous QPR and presented in Table 2.4.b below.

The two damage scenario cases selected above consisted of removing the entire external web of one box which may model the effect of major damage as consequence of an impact with the box. Other damage scenarios would be investigated in the section of parametric analysis.

The above analysis assumes that a single lane is loaded by one lane of HS-20 truck. The same analyses performed above are repeated assuming that the bridge is loaded by two lanes of HS-20 trucks. For this particular bridge, with R=179,577 kip-in, DL= 53,081 kip-in and $DF_1$ $LL_{HS-20}$ =11,237 kip-in, the first member failure assuming linear elastic behavior occurs at $LF_1$= (179577-53081)/11,237=11.26. The results of the push-down analysis are illustrated in Figure 2.10. The nonlinear analysis leads to $LF_f$ =10.33, $LF_u$=11.21 and $LF_d$=7.11 for the damage scenario where the entire external web is removed. The results are shown in the second row of Table 2.4.a.

From Table 2.4.a, we can see that the spread box bridge will have no redundancy for the ultimate limit state if the bridge is loaded by two lanes of trucks. This is because the two boxes are essentially equally loaded and they both reach their ultimate capacities together. These results are consistent with those observed for steel box-girder bridges. Table 2.4.b shows the results obtained in the previous QPR for the steel spread box girder bridge.

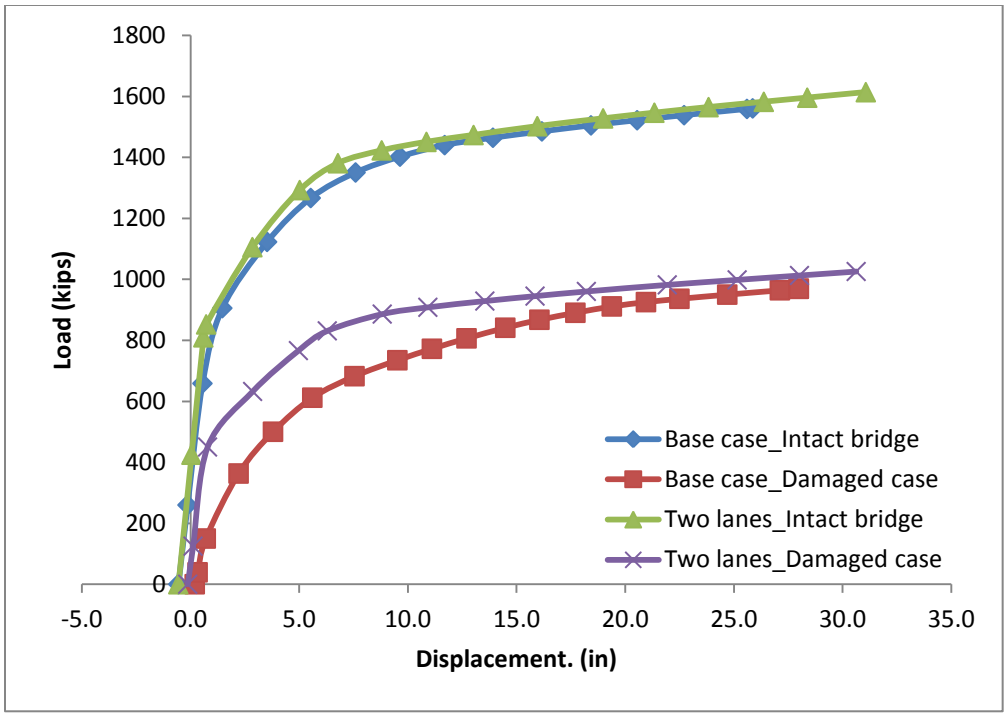


**Figure 2.10 Load-displacement curves of one-lane and two-lane loading bridges**

**Table 2.4.a Comparison of results of redundancy ratios for spread prestressed box bridge**

| 120 ft. simple span | $LF_1$ | $LF_{100}$ | $LF_u$ | $LF_d$① | $R_{f100}$ | $R_u$ | $R_d$① |
|---|---|---|---|---|---|---|---|
| One lane loaded(Base case) | 18.05 | 20.40 | 21.68 | 13.46 | 1.13 | 1.20 | 0.74 |
| Two lanes loaded | 11.26 | 10.33 | 11.21 | 7.11 | 0.92 | 1.00 | 0.63 |

Note: ① represent the damage case 1.

**Table 2.4.b Comparison of results of redundancy ratios for spread steel box bridge**

| 120 ft. simple span | $LF_1$ | $LF_{100}$ | $LF_u$ | $LF_d$ | $R_{f100}$ | $R_u$ | $R_d$ |
|---|---|---|---|---|---|---|---|
| One lane loaded | 11.26 | 12.98 | 14.08 | 8.38 | 1.15 | 1.25 | 0.74 |
| Two lanes loaded | 7.56 | 7.40 | 7.48 | 5.36 | 0.98 | 0.99 | 0.71 |

# 3. Parametric Analysis

## 3.1 Effect of boundary conditions

In the grillage model of the base case, we assume that each box is supported by two end bearings lined up below each web of the box. This model assumes pin supports at the end of each longitudinal beam as shown in Figure 3.1.a. If only one bearing is set under each box, it is necessary change the boundary conditions for the new case (Case 1) and place the pin supports at the midpoint of the box as shown in Figure 3.1.b. To accommodate that position, we also assume that there is a diaphragm at the end of each box. In summary, the two cases for the end conditions compared in this section are:

Base Case - Pins are applied below each web (Figure 3.1.a);
Case 1 - Diaphragms are applied at the ends of each box and one pin is applied below the midpoint of each box (Figure 3.1.b).

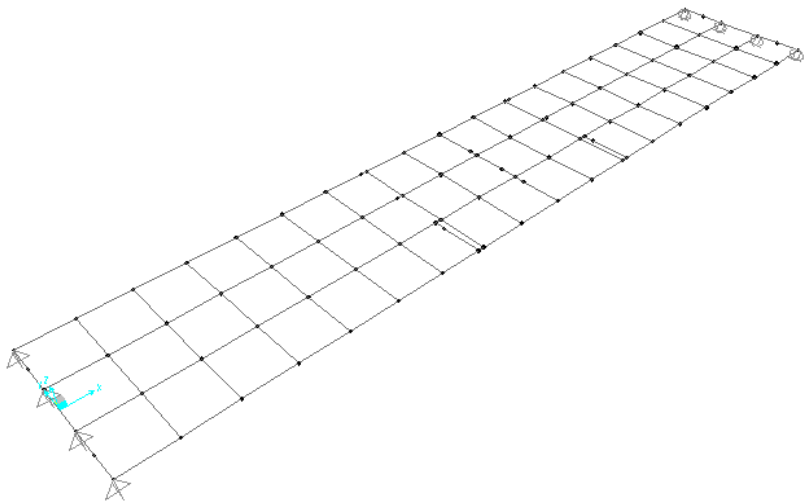

(a) Base case

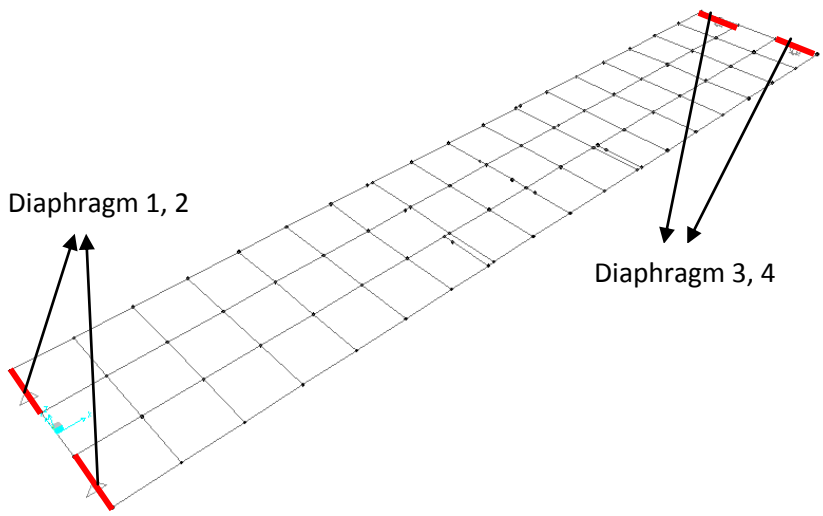


(b) Case 1

**Figure 3.1 Boundary conditions for different number of bearings**

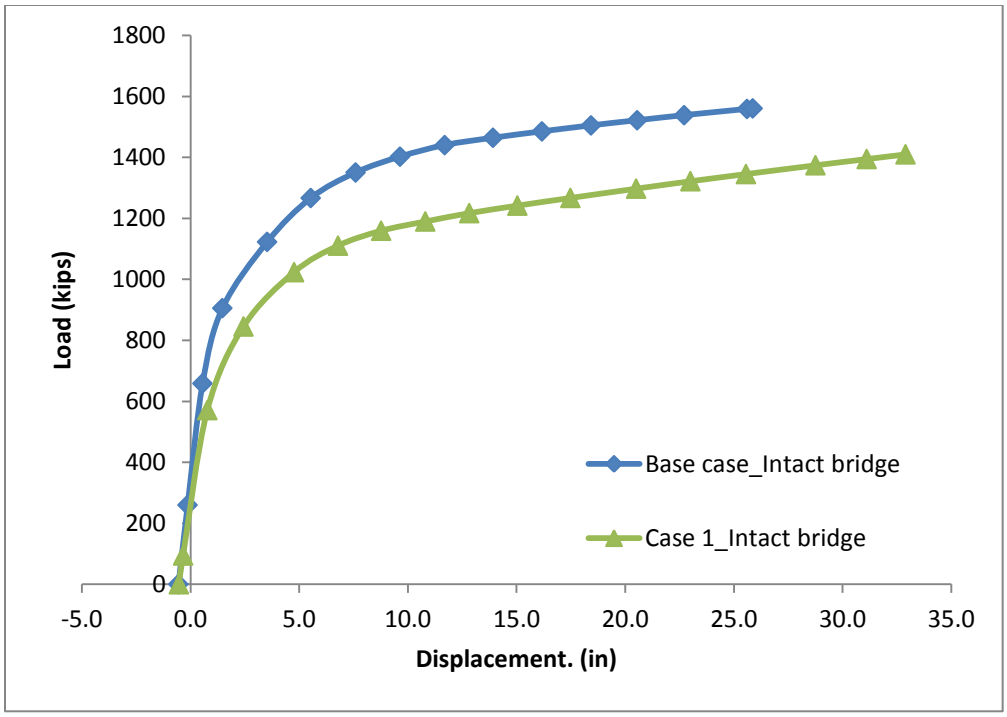


**Figure 3.2 Load-displacement curves for different bearings**

The ultimate capacities for Base case and Case 1 are found when the total applied live load is respectively equal to1,560.9 kips and 1,410.2 kips. The moment capacity and load moments of the external longitudinal beam (one half composite box) in SAP 2000 models are listed in Table 3.1.

Base case: R=179,577 kip-in, DL= 53,081 kip-in, LL=7,008 kip-in;

Case 1: R=179,577 kip-in, DL= 53,081 kip-in, LL=7,790 kip-in;

The corresponding load factors $LF_1$ for the first member failure for the Base case and Case 1 are found to be 18.05 and 16.24, respectively, as summarized in Table 3.1.

**Table 3.1 Comparison of results of redundancy ratios for different bearings**

| 120 ft. simple span | $LF_1$ | $LF_{100}$ | $LF_u$ | $R_{f100}$ | $R_u$ |
|---|---|---|---|---|---|
| Base case | 18.05 | 20.40 | 21.68 | 1.13 | 1.20 |
| Case 1 | 16.24 | 17.15 | 19.59 | 1.06 | 1.21 |

From Table 3.1, we can see that the load factors $LF_1$ and $LF_u$ of Case 1 with one pin under each box decrease compared to those of the Base case. The reason is that when the pin is applied at the middle of the box it will lead to larger box rotations as compared to the case when a pin support is applied under each web. This additional rotation produces a larger deflection of the external box and reduces the load that is transferred to the other box, as shown in Figure 3.2. However, the bearing condition does not change the bridge redundancy for the ultimate limit state because the percentage change in the linear elastic response and the ultimate response are essentially similar. Thus, the redundancy ratio $R_u$ remains essentially the same.

## 3.2 Effect of damage of prestressing steel and reduction in member capacity

### 3.2.1 Damage to the external box only

The damage scenario selected the in Base case consisted of removing the entire external web of one box which may model the effect of major damage due to overall deterioration or as consequence of an impact with the box. Another damage scenario for prestressed concrete box girders consists of modeling corrosion of prestressing steel. In this section, the analysis is performed assuming that the external box loses some percentage of the strands along the whole span. In this alternate damage scenario, we assume different percent loss in the number of strands and the box keeps the torsional capacity of the closed section. The analysis of the bridge shows a linear relationship between the redundancy ratios and percentage of damaged strands. The redundancy ratios decrease with the increasing percentage of damaged tendons. We can further conclude that the allowable percentage of damaged tendons of the external box should not exceed 79% in order to satisfy the minimum $R_d$=0.5 criterion proposed in NCHRP 406. The cases we analyzed are listed as follows:

Base Case: The entire external web is damaged and removed from the bridge model;
Case 1: The two webs of the loaded box are the same but lose 50% of the tendons;
Case 2: The two webs of the loaded box are the same but lose 60% of the tendons;
Case 3: The two webs of the loaded box are the same but lose 80% of the tendons.

Moment curvature curves for the Base Case and Cases 1 through 3 are shown in Figure 3.3. Variations in the percentage of damaged tendons change the moment-curvature relationship of the damaged prestressed box girder. Figure 3.4 shows the SAP2000 model used for the damaged scenario for Cases 1 through 3. The load deflection curves for the Base case and Cases 1 through 3 are shown in Figure 3.5. The redundancy ratios are summarized in Table 3.2.

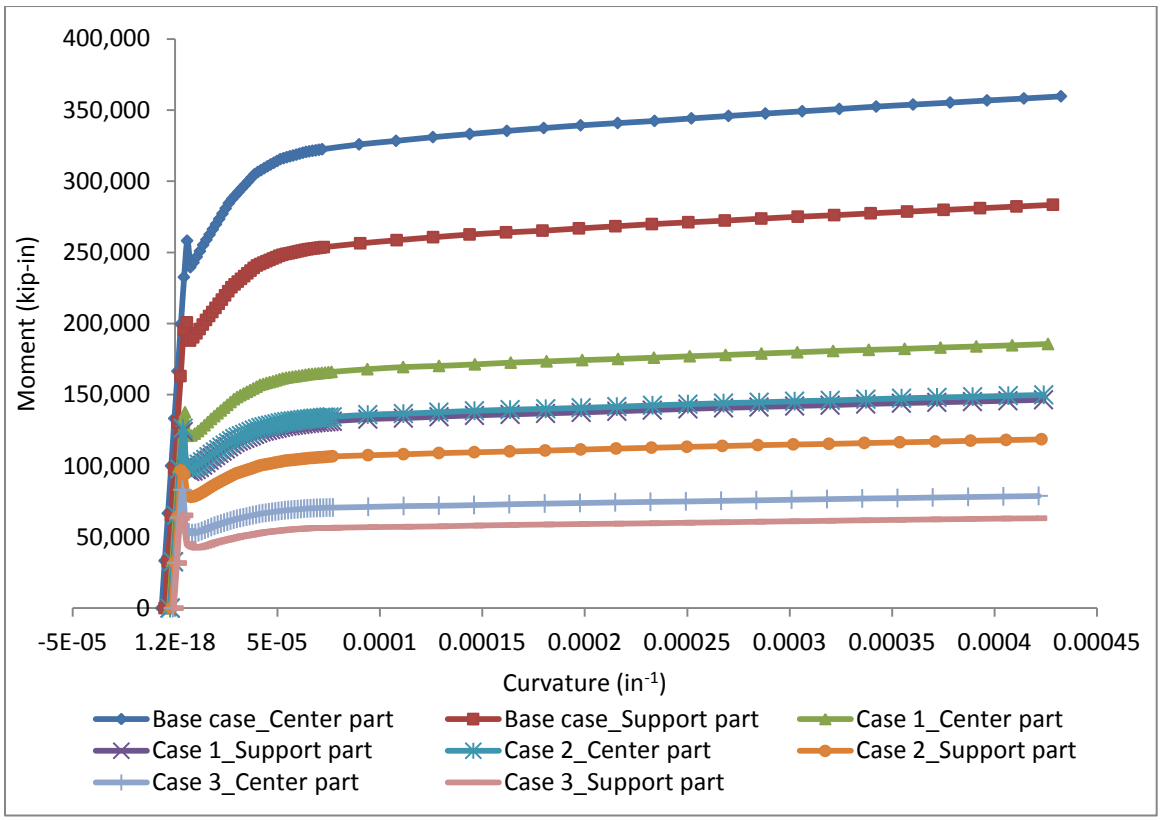


**Figure 3.3 Moment curvature curves of Base Case and for different losses in prestressing for one box from Xtract program**

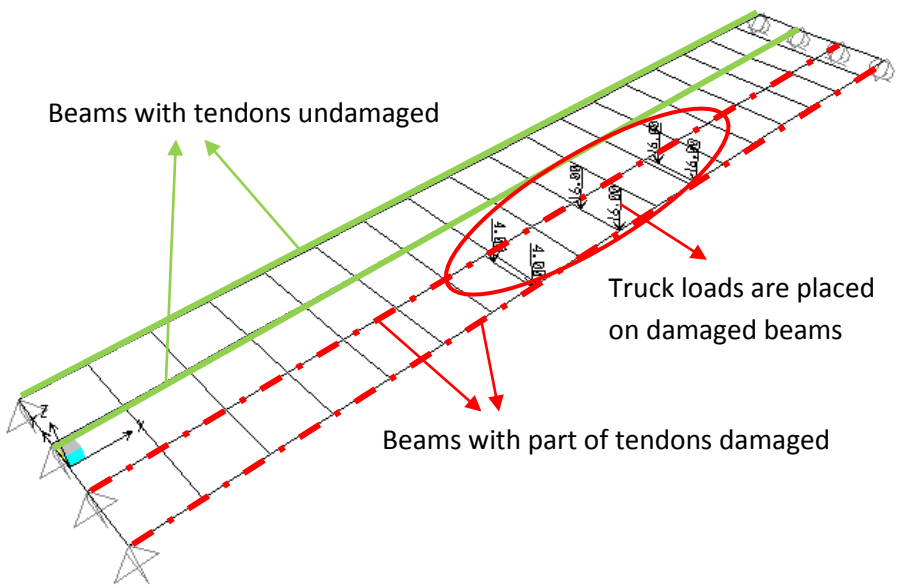


**Figure 3.4 Two types of beams in the SAP model for the damaged scenario for Cases 1-3**

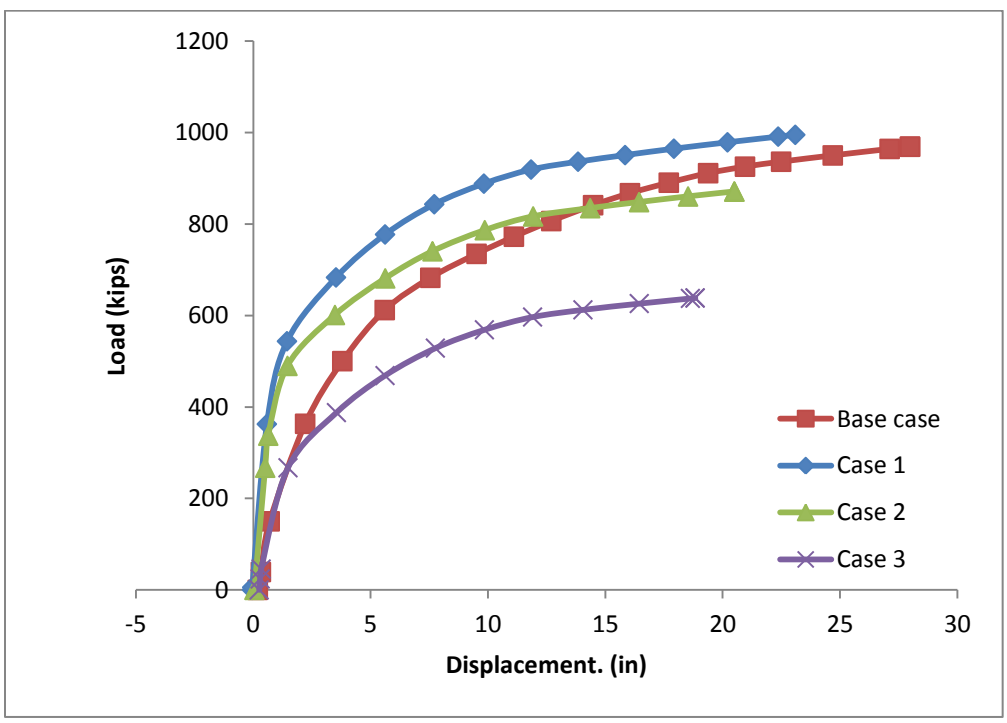


**Figure 3.5 Load deflection curves for the damaged scenario for different losses in prestressing tendons**

The analysis of the damaged bridge scenarios shows that the ultimate capacities for the Base case, Case 1, Case 2 and Case 3 are reached when the applied live load reaches $LF_d$= 969.2 kips, 995.2 kips, 871.0 kips and 638.5 kips, respectively, as shown in Figure 3.5.

Comparing $LF_d$ for all the damage scenarios including the Base case and Cases 1 through 3, to the load factor $LF_1$=18.05 which is the load at which the first member fails assuming linear elastic behavior of the undamaged bridge, we obtain the results summarized in Table 3.2. Figure 3.6 shows a plot of the linear relationship between the redundancy ratio $R_d$ and the percentage of damaged tendons. The base case is shown as the red triangle.

**Table 3.2 Comparison of results of redundancy ratios for different losses in prestressing tendonds**

| 120 ft. simple span | $LF_1$ | $LF_d$ | $R_d$ ① |
|---|---|---|---|
| Base case | 18.05 | 13.46 | 0.74 ① |
| Case 1 | 18.05 | 13.82 | 0.76 |
| Case 2 | 18.05 | 12.10 | 0.67 |
| Case 3 | 18.05 | 8.87 | 0.49 |

Note: ① represent the damaged scenario 1 mentioned in Section 2.2.

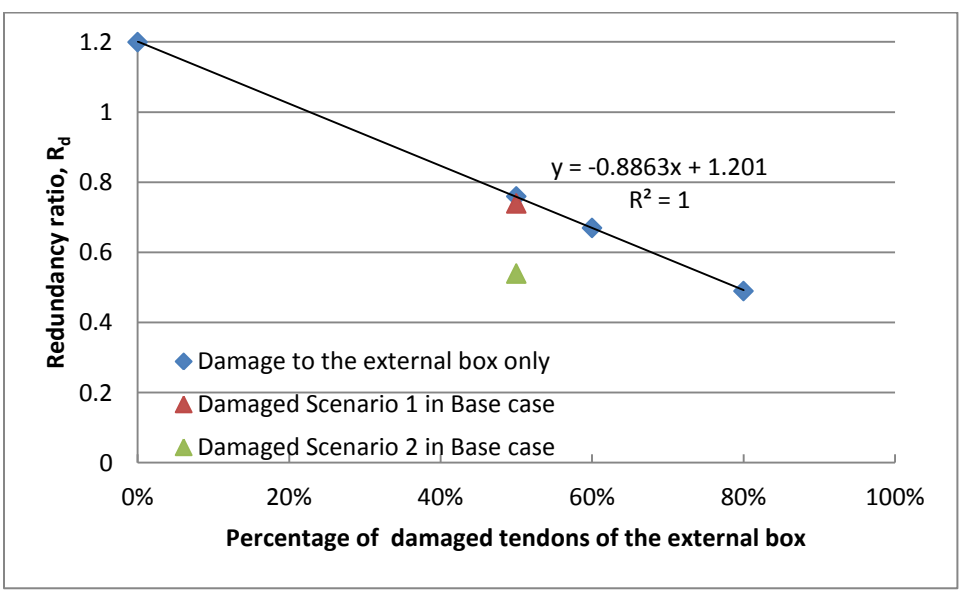


**Figure 3.6 Relationship of redundancy ratio $R_d$ and percentage of damaged tendons**

From Table 3.2 and Figure 3.6, we can see that the redundancy ratio decreases linearly with the increasing percentage of damaged tendons. Also, the redundancy ratio $R_d$ of Case 1 is very close to the value of the damaged case 1 in Base case where the external beam is removed but the torsional constant of the adjacent web is not affected, which is reasonable because in both damage scenarios the loss is about 50% of the box capacity although in the base case, the damage is completely attributed to the external web while in the analysis performed in this section the two webs are equally reduced. The difference in the way the reduction is distributed leads to different load deflection curves although the overall capacities are similar as shown in the red and blue curves in Figure 3.5. The overall capacities remain essentially the same whether the reduction is concentrated in one web or spread to both webs is due to the high torsional property of the box which spread the load equally to the entire box when the load approaches failure. As mentioned earlier, if the torsion of the box is drastically reduced say due to shear failure of the external web, there will be a 29% reduction in the redundancy ratio $R_d$ because of the box becomes an open section with a significantly reduced torsional constant. Also, from Figure 3.6, we can clearly see that the redundancy ratio $R_u$ which is equal to 1.2 when none of the tendons are damaged lines up very well with the damaged cases analyzed in this section.

According to the equation of the linear trend-line in Figure 3.6, we can conclude that the allowable percentage of damaged tendons of the external box analyzed in this section should not exceed 79% in order to satisfy the minimum $R_d$=0.5 criterion proposed in NCHRP 406.

### 3.2.2 Reduction in capacity of two boxes

In Section 3.2.1, we performed the redundancy analysis of bridges on the assumption that only the external box loses some percentage of the strands along the whole span. In this section, we still assume different percent loss in the number of strands but we assume that the loss is in both of the two boxes. The analysis of the bridge also shows a linear relationship between the redundancy ratios and percentage of damaged strands. Naturally, the ratios decrease much more rapidly with the increasing percentage of damaged tendons in both boxes as compared to the case with only the external box damaged. We can

further conclude that the allowable percentage of damaged tendons in each box should not exceed 42% to satisfy the minimum $R_d$=0.5 criterion proposed in NCHRP 406. The cases we analyzed are listed as follows:

Base Case: No tendons lost;

Case 1: Each of the two boxes loses 50% of the tendons;

Case 2: Each of the two boxes loses 60% of the tendons;

Case 3: Each of the two boxes loses 80% of the tendons.

Moment curvature curves for the Base Case and Cases 1 through 3 are the same as those described in Section 3.2.1. Figure 3.7 shows the SAP2000 model used for the damaged scenario for Cases 1 through 3. The load deflection curves for the Base case and Cases 1 through 3 are shown in Figure 3.8. The redundancy ratios are summarized in Table 3.3.

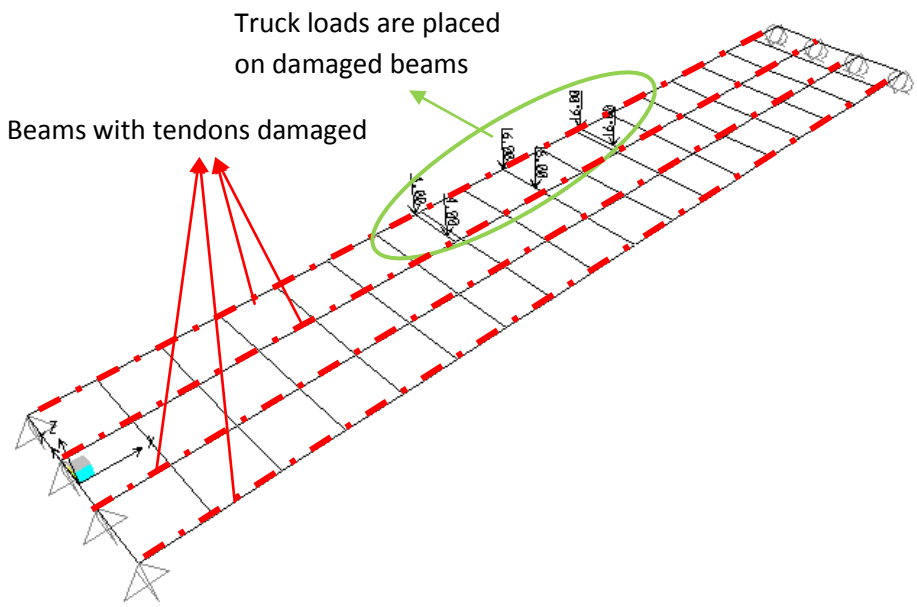


**Figure 3.7 Damaged beams in the SAP model for the ultimate limit state of Case 1-3**

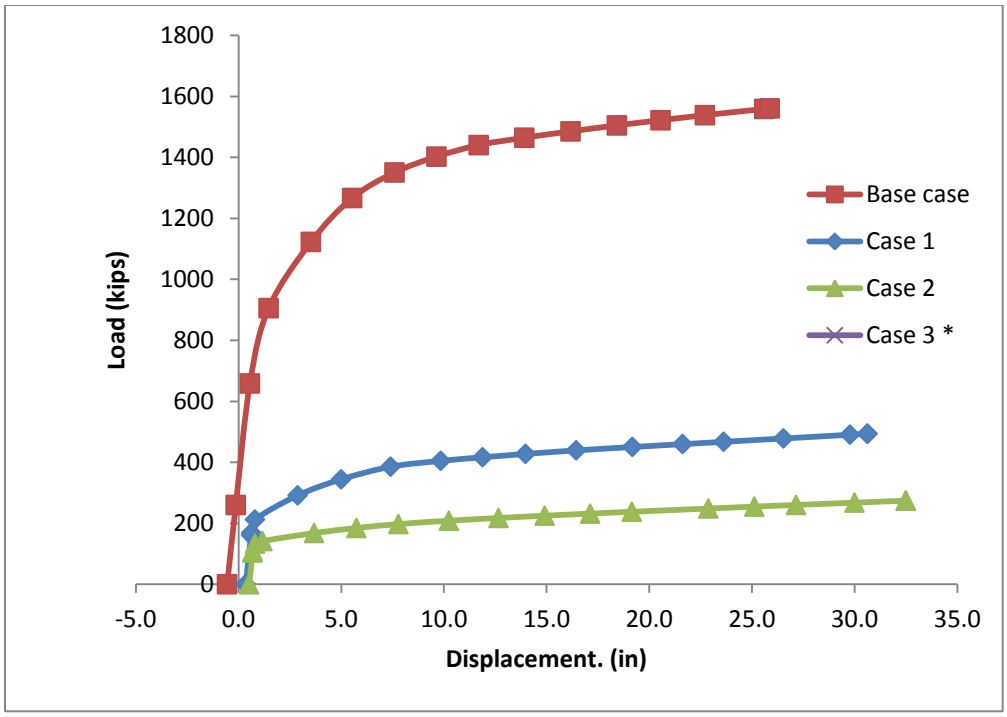


Note: * The bridge fails under its self weight in Case 3.

**Figure 3.8 Load deflection curves when both boxes are damaged**

The analysis of the damaged bridge scenario shows that the ultimate capacities for Base case, Case 1 and Case 2 are reached when the applied live load reaches 1,560.9 kips, 493.9 kips, and 274.4 kips, respectively, as shown in Figure 3.5. In Case 3, as the bridge cannot hold the self-weight, so there is no capacity for live load. The results for $R_d$ as summarized in Table 3.3 are relative to the linear elastic behavior represented by $LF_1$ for the original bridge with the full capacity of the boxes.

**Table 3.3 Comparison of results of redundancy ratios for the cases when both boxes are damaged**

| 120 ft. simple span | $LF_1$ | $LF_d$ | $R_d$ |
|---|---|---|---|
| Base case | 18.05 | 21.68 | 1.20 |
| Case 1 | 18.05 | 6.86 | 0.38 |
| Case 2 | 18.05 | 3.81 | 0.21 |
| Case 3 | 18.05 | -- | -- |

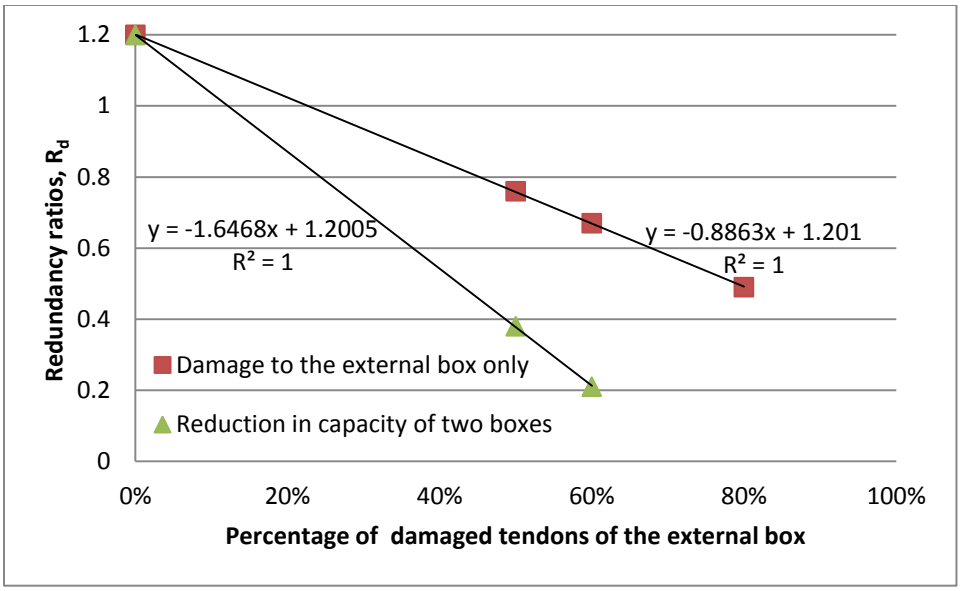


**Figure 3.9 Comparison of relationships of redundancy ratio and percentage of damaged tendons for the two-box damaged scenarios**

From Table 3.3 and Figure 3.9, we can see that the redundancy ratio $R_d$ decreases with the increasing percentage of damaged tendons, whose relationship is linear like that of the of the one-box damaged scenarios. However, the decreasing slope in the case of two boxes damaged is 1.86 times that of the one-box damaged scenarios.

According to the equation of the linear trend-line of the two damaged scenarios in Figure 3.9, we can conclude that the allowable percentage of damaged tendons of the external box should not exceed 79% and 42% for the one-box and two-box damaged scenarios respectively, in order to satisfy the redundancy criterion $R_d$=0.5.

## 3.3 Analysis of continuous bridges

To study the effect of span continuity, the redundancy of a three-span continuous bridge (80 ft-120 ft-80 ft) is compared to that of the 120-ft simple span bridge. The three-span prestressed concrete superstructure is designed to be simple-supported for dead load but continuous for live load.

The continuous twin prestressed concrete box bridge sections have the same dimensions as the box described in Section 2.1 and shown in Figure 2.4. The negative bednign region is assumed to have regular reinforcement and designed to carry the AASHTO negavtive bending moment for live load. The positive and negative moment capacities as well as the equivalent end moments applied to adjust the Moment-curvature relationship to account for the effect of the moments in the blanketed and fully bonded regions are listed in Table 3.4. In the next section, we analyze the effect of different positive and negative moment capacities. The moment-curvature relationships for the positive bending and negative bending regions for the sections with the capacities shown in Table 3.4 are shown in Figure 3.10 and Figure 3.11, respectively.

**Table 3.4 Equivalent moments of the continuous prestressed concrete box bridge**

| Items | Base case (120-ft simple span bridge) | Case 1 (80 ft-120 ft-80 ft continuous bridge) | |
|---|---|---|---|
| | 120-ft span | 120-ft span | 80-ft span |
| $R^+$ | 179,577 | 179,577 | 79,812 |
| $R^-$ | -- | 53,600 | |
| $M_1$ (kip-in.) | 53,426 | 53,426 | 23,713 |
| $M_2$ (kip-in.) | 17,101 | 17,101 | 7,931 |

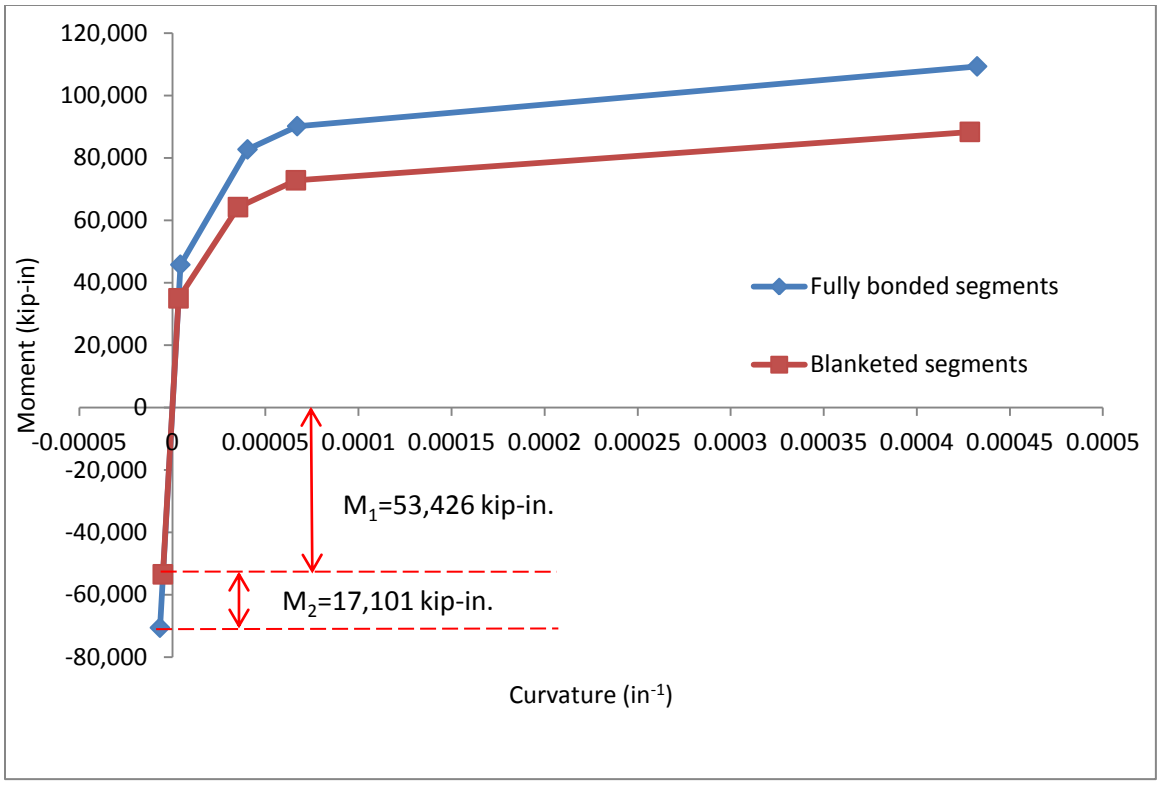


**Figure 3.10 Moment curvature curves for positive bending for the mid-span of the continuous bridge**

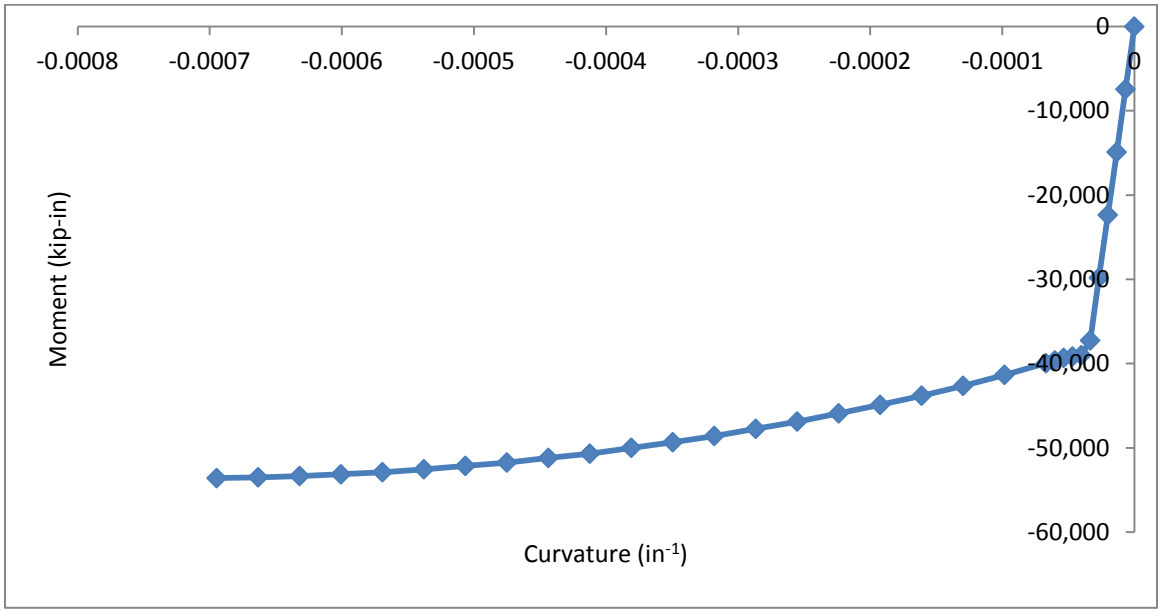


**Figure 3.11 Moment curvature curve for negative bending region**

The SAP2000 model of the three-span continuous steel box girder bridge is developed as shown in Figure 3.12. The load deflection curves of the ultimate limit state and the damaged scenario for the continuous bridge (labeled Case 1) are compared to those of the simple span bridge (labeled Base Case) are shown in Figure 3.13. The redundancy ratios for the continuous bridge are summarized in Table 3.5. Here again, the two damaged scenarios where one damaged box is assumed to maintain its torsional capacity while losing its strength is compared to the case where the box loses also its torsional capacity. The results are compared to the results of the 120-ft simple span bridge analyzed in Section 2.2.

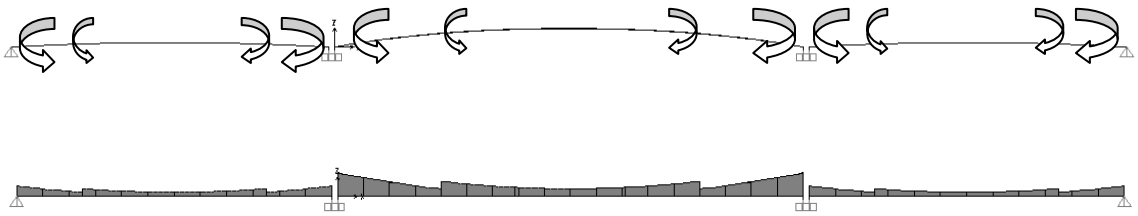

(1) Deformed shape and moment diagram of simple supported bridges duo to dead load including prestressing forces

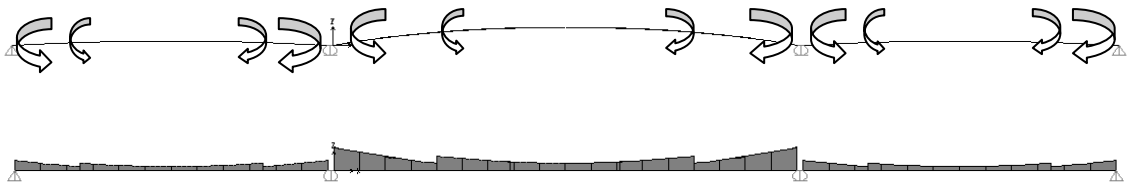

(2) After concrete construction joint are hardened, temporary bearings are removed and replaced by permanent ones, then the bridge is continuous to live load

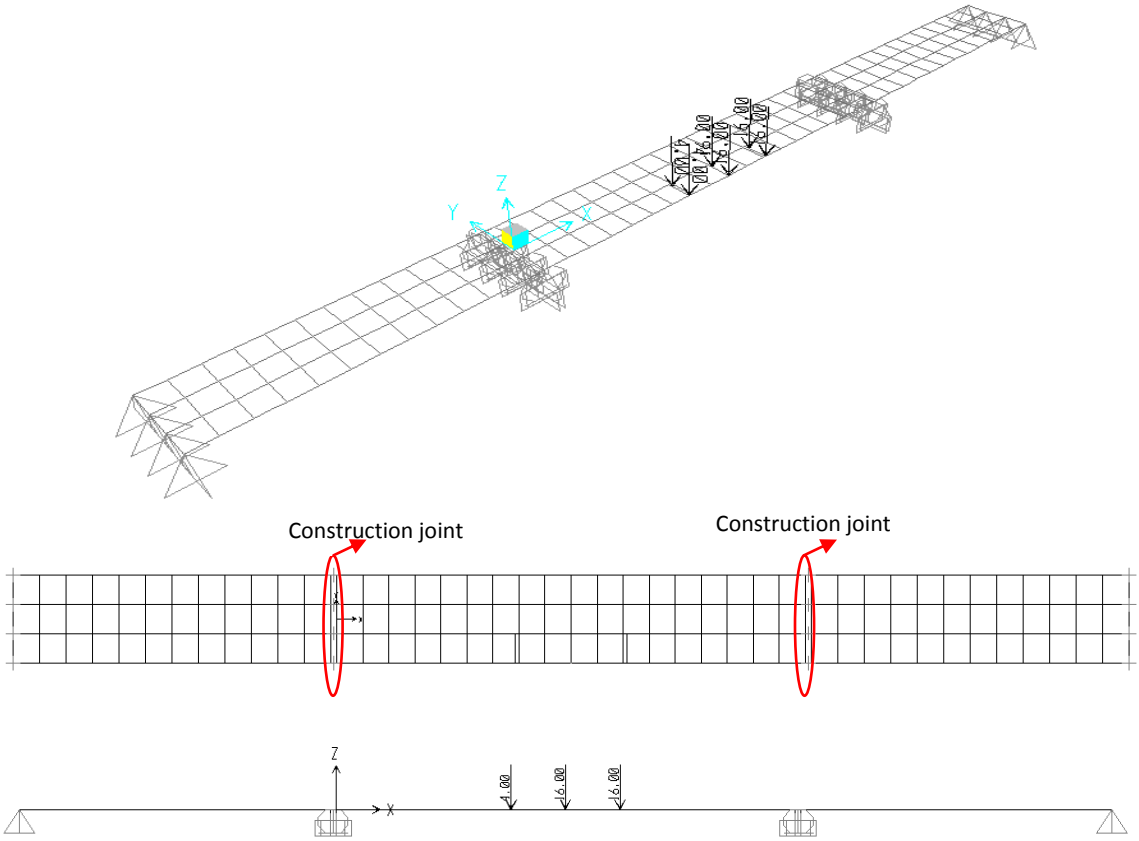


(3) HS-20 truck loads are placed on the continuous bridge

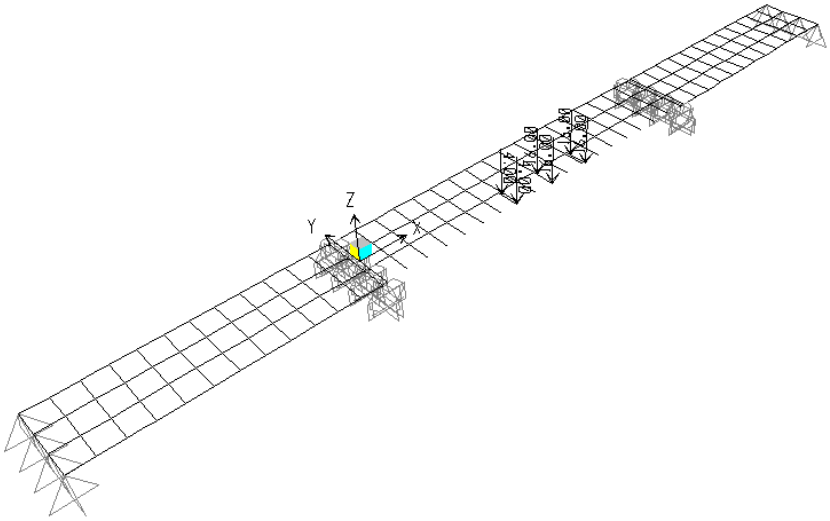

(4) Damaged limit state

**Figure 3.12 SAP2000 model of the three span continuous prestressed concrete bridge**

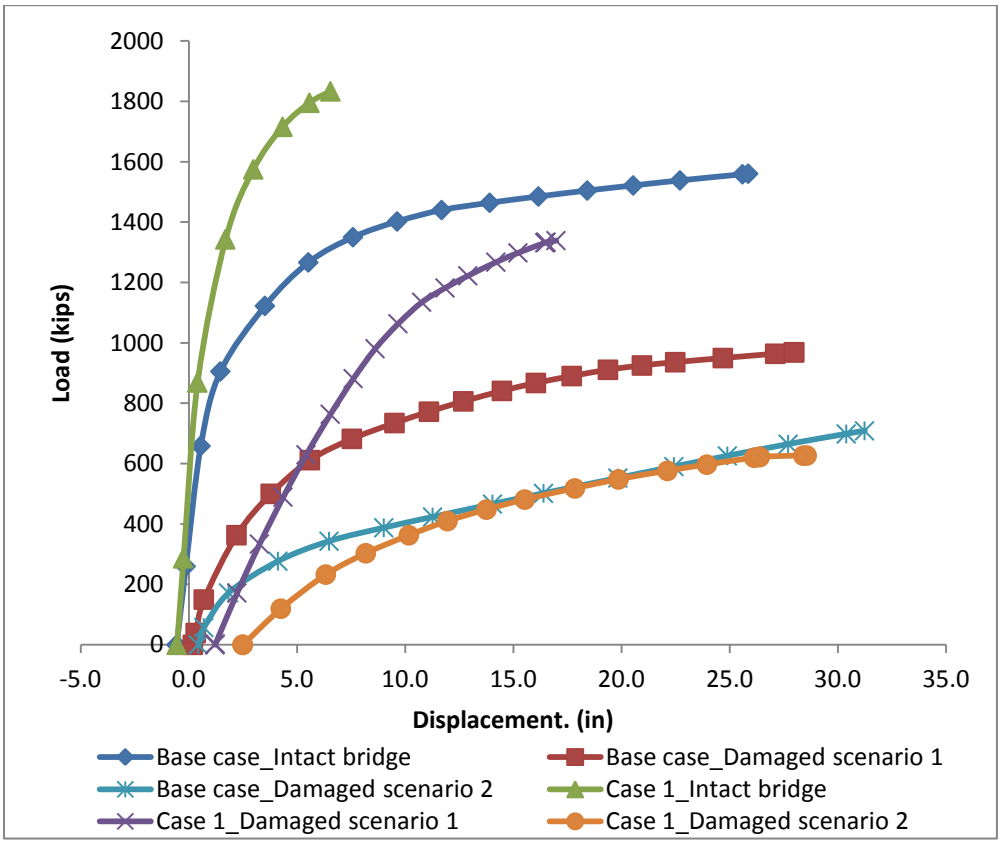


**Figure 3.13 Load deflection curves of simple span (base case) and continuous bridge.**

The ultimate capacities for the simple span bridge case and the continuous bridge are found when the total applied live load is respectively equal to 1,560.9 kips and 1,833.8 kips, as shown in Figure 3.13. The analysis of damage scenario 1 shows that the ultimate capacities are reached when the applied live load reaches 969.2 kips and 1,339.3 kips for the simple span case and continuous bridge, respectively. The analysis of damaged scenario 2 shows that the applied live load reaches 709.0 kips and 627.0 kips for the simple span case and continuous bridge. The results of the analysis are summarized in Table 3.5.

The moment capacity and load moments of the external longitudinal beam (one half composite box) in SAP 2000 models are listed as follows.

Simple span: R=179,577 kip-in, DL=53,081kip-in, LL=7,008 kip-in;

Continuous bridge: R=179,577 kip-in, DL=53,081kip-in, LL=5,324 kip-in;

The corresponding load factors $LF_1$ for first member failure for the simple span case and the continuous bridge are found to be 18.05 and 23.76, respectively, as summarized in Table 3.5.

**Table 3.5 Comparison of results of redundancy ratios**

| Cases | $LF_1$ | $LF_u$ | $LF_d$① | $LF_d$② | $R_u$ | $R_d$① | $R_d$② |
|---|---|---|---|---|---|---|---|
| Simple span | 18.05 | 21.68 | 13.46 | 9.85 | 1.20 | 0.74 | 0.54 |
| Continuous | 23.76 | 25.47 | 18.60 | 8.71 | 1.07 | 0.78 | 0.37 |

Note: ① and ② represent the damage scenario 1 and 2 in Section 2.2, respectively.

From Table 3.5, it is observed that this continuous bridge made by simple supported bridges has slightly lower redundancy ratios for both the ultimate limit state and damaged scenario 2 than those of the simple span bridge (Base case). This is because, the $LF_1$ load is increased significantly with a decreasing live load moment of the continuous bridge, while the ultimate capacities for the intact and damaged bridges are not increased as much. However, the continuous bridge has a little higher redundancy ratio than that of the simple bridge in the damage scenario 1 without a torsional capacity loss. Comparing the redundancy ratios in the damage scenario 1 and 2, we can find the loss in the torsional capacity has a significant effect on the behavior of continuous bridges. We will see that the bridge redundancy ratios of continuous bridges are also dependent on the positive moment capacities of the longitudinal beams as well as the negative bending moment capacities. These effects are investigated in Section 3.4.2.

## 3.4 Effect of dead load and member strength capacity

### 3.4.1 Simple supported bridge

In this section we analyze the effect of the resistance on the redundancy of the 120-ft simply supported prestressed concrete box girder bridge. The results of the analysis for both of the ultimate limit state and damaged scenario are summarized in Table 3.6. Several cases are analyzed consisting of changing the dead load moment by up to +/- 40%. Also, the moment capacity of the 120-ft simple span bridge is changed by - 50% and - 60%. The results show minor changes in the redundancy ratio for the ultimate limit state, $R_u$ which varies between a maximum value of $R_u$=1.22 and a minimum value of $R_u$=1.17 even though the moment capacity and dead load change by up to 60% and 40%, respectively. This observation confirms that the redundancy ratio $R_u$ is not sensitive to changes in the member capacities or the dead load intensities for simple span bridges. However, the changes in member resistances will have some effect on the redundancy ratios for the damaged limit state. The results show that the redundancy ratio $R_d$ decreases as the member resistance decreases by a percentage on the order of about 60% of the change in member capacity. Although the redundancy ratio for the damage case decreases when the dead load is increased, the effect of the dead load on the damaged is less significant than that of the resistance. The change in dead load by 40% leads to a reduction in $R_d$ of less than 7%. The above observations are consistent with those of the simple span bridges with composite steel I-girders. In this set of analyses for the damaged state scenario we have assumed that the dead load of the damaged beam is transferred to the adjacent beams. More specific information is provided next.

**(1) Only resistance changed**

The analysis is performed assuming that the moment capacity of the boxes is changed from the value in the Base case for the two boxes of the bridge. The cases we analyzed are listed as follows:

Case 1: Moment capacity - 50%; Elastic section stiffness is the same as that of Base case;
Case 2: Moment capacity - 60%; Elastic section stiffness is the same as that of Base case;

Figure 3.14 gives the total reactions versus the maximum vertical deflection of the bridge when a nonlinear incremental load analysis is performed. The results of the pushdown analysis are summarized in Table 3.6.

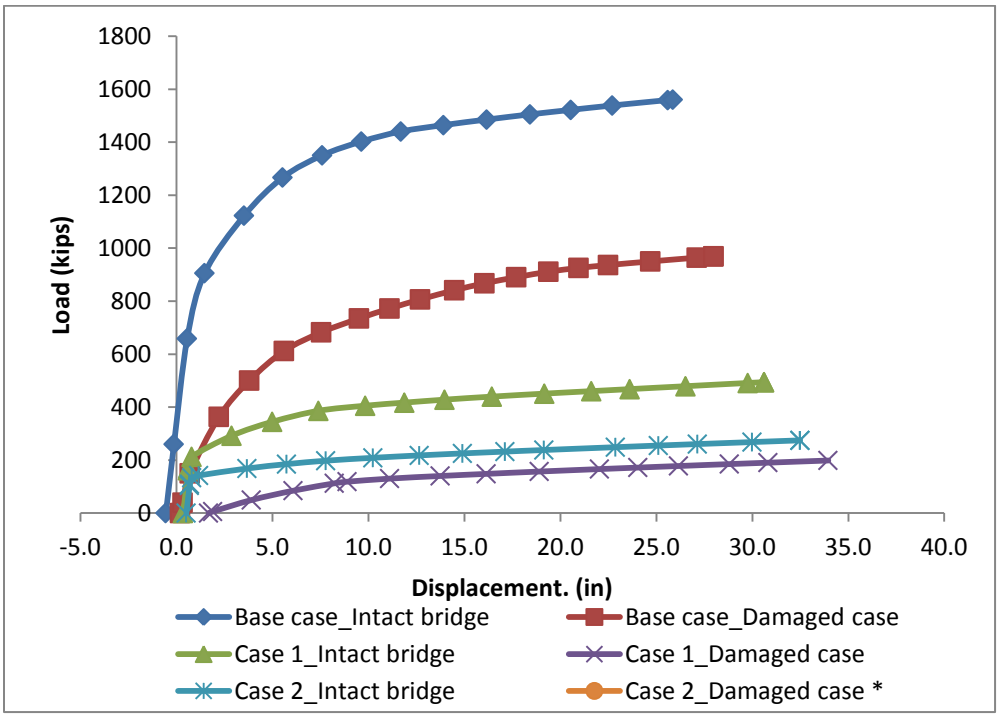


Note: * The bridge fails under its dead load.

**Figure 3.14 Load deflection curves of Base case and Cases 1-2 for both of the ultimate limit state and the damaged scenario for different member strengths**

The load deflection curves for the Base case and Cases 1 and 2 show a reduction in the live load capacity from 1,560.9 kips to respectively 493.9 kips and 274.4 kips. The analysis of the damaged bridge shows that the ultimate capacities are reached when the applied live load are 969.2 kips, 206.8 kips for the Base case and Case 1. The bridge fails under its dead load for Case 2.

**(2) Only dead load changed**

The analysis is performed assuming that the dead load of the boxes is changed from the value of the Base case. The cases we analyzed are listed as follows:

Case 1: Dead load + 10%

Case 2: Dead load + 20%

Case 3: Dead load + 40%

Case 4: Dead load - 10%

Case 5: Dead load - 20%

Case 6: Dead load - 40%

The load deflection curves of the ultimate limit state and the damaged bridge scenario for the Base case and Cases 1 through 6 are shown in Figure 3.15 and Figure 3.16, respectively. The redundancy ratios are also summarized in Table 3.6. The damage scenario considered assumed that the torsional constant is not changed when the external web capacity is reduced so that the external box loses half its strength.

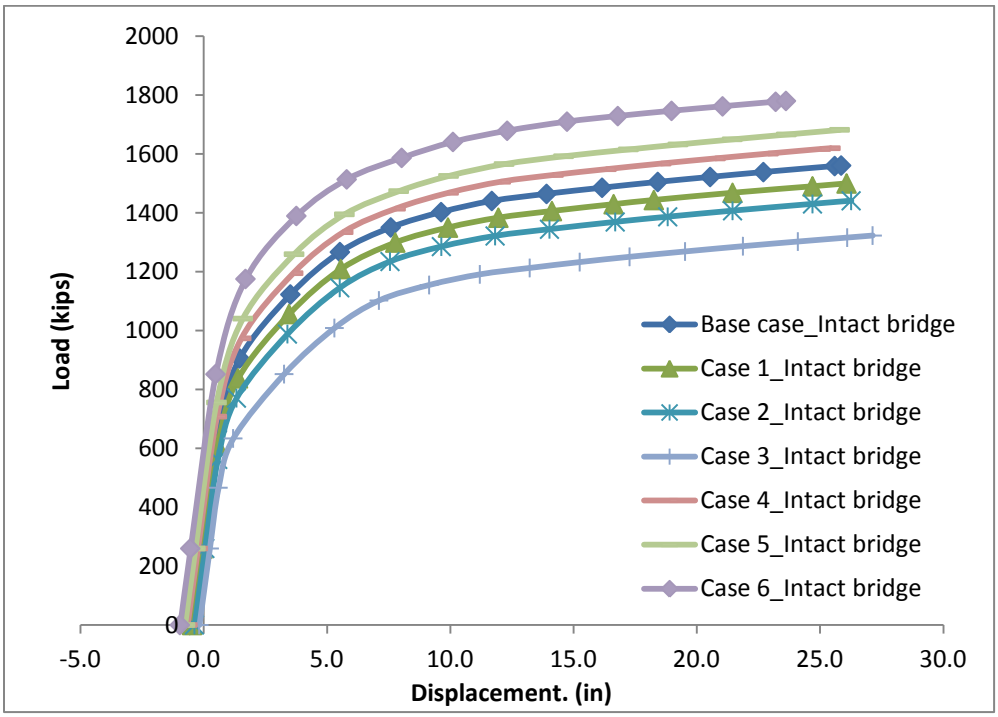


**Figure 3.15 Load deflection curves of Base case and Cases 1-6 for the ultimate capacity for different dead loads**

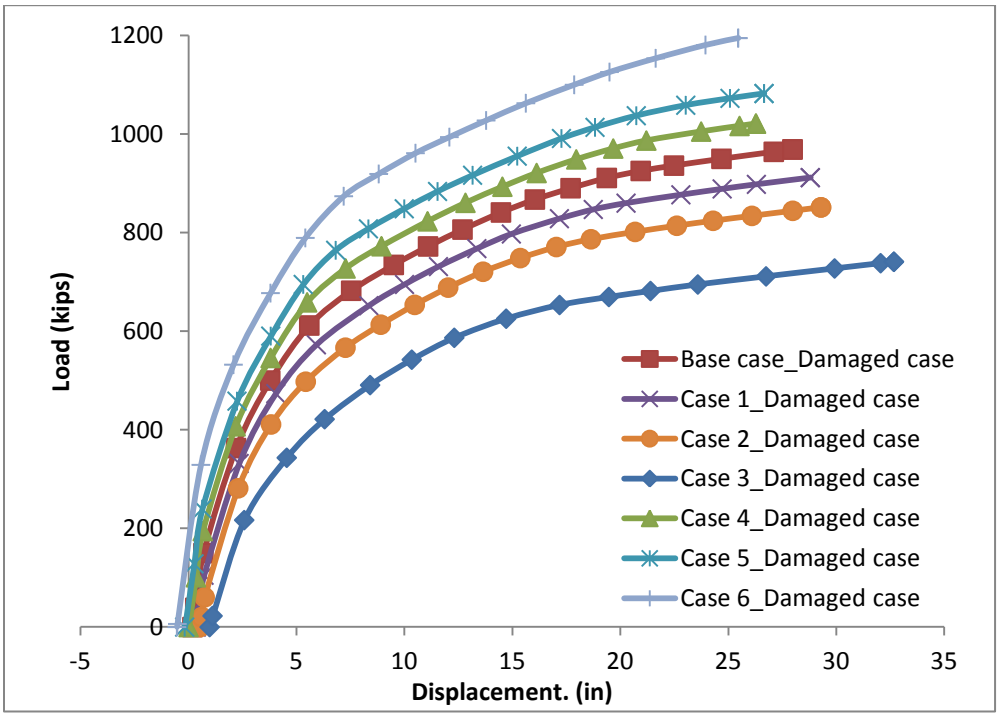


**Figure 3.16 Load deflection curves of Base case and Cases 1 through 6 for the damaged scenario for different dead loads**

The ultimate capacities for the Base case and Cases 1 through 6 correspond to a total applied live load varying from 1,560.9 kips to respectively 1,500.0 kips, 1,441.1 kips, 1,323.0 kips, 1,619.8 kips, 1,682.3 kips and 1,780.3 kips. The analysis of the damaged bridge scenario shows that the ultimate capacities are reached when the applied live load reaches 969.2 kips, 911.9 kips, 851.6 kips, 741.2 kips, 1,021.5 kips, 1,082.6 kips and 1,195.2 kips.

**Table 3.6 Summary of results for simple span bridges with different R and D values**

| Cases | R (ft-in) | D (ft-in) | $LF_1$ | $LF_u$ | $LF_d$① | $R_u$ | $R_d$① |
|---|---|---|---|---|---|---|---|
| Base case | 179,577 | 53,081 | 18.05 | 21.68 | 13.46 | 1.20 | 0.74 |
| Case 1 | 92,800 (-50%) | 53,081 (--) | 5.67 | 6.86 | 2.87 | 1.21 | 0.51 |
| Case 2 | 74,950 (-60%) | 53,081 (--) | 3.12 | 3.81 | 3.08 | 1.22 | --* |
| Case 1 | 179,577 (--) | 58,389 (+10%) | 17.29 | 20.83 | 12.66 | 1.20 | 0.73 |
| Case 2 | 179,577 (--) | 63,697 (+20%) | 16.54 | 20.02 | 11.83 | 1.21 | 0.72 |
| Case 3 | 179,577 (--) | 74,313 (+40%) | 15.02 | 18.38 | 10.29 | 1.22 | 0.69 |
| Case 4 | 179,577 (--) | 47,773 (-10%) | 18.81 | 22.50 | 14.19 | 1.20 | 0.75 |
| Case 5 | 179,577 (--) | 42,465 (-20%) | 19.57 | 23.36 | 15.04 | 1.19 | 0.77 |
| Case 6 | 179,577 (--) | 31,849 (-40%) | 21.08 | 24.73 | 16.6 | 1.17 | 0.79 |

Note: ① represents the damage case 1 mentioned in Section 2.2.

*: The bridge fails under its dead load.

### 3.4.2 Three-span continuous bridge

In this section we analyze the effect of changes in the bending moment capacity for the three-span continuous bridge. The analysis is performed for the continuous bridge with three spans at 80 ft-120 ft-80 ft. The analysis is performed for the narrow bridge configuration with one lane loaded. The continuous bridge has four longitudinal beams representing the webs of two prestressed concrete boxes at 14 ft-9 in. spacing. The results of the analysis for the ultimate limit state and damaged scenario are summarized in Table 3.7. Several cases are analyzed consisting of changing the moment capacity of the continuous bridge as follows:

**(1) Only negative bending capacity is changed**

The analysis is performed assuming that the negative moment capacity for the reinforced beam section in the support region is changed from the value originally used. The cases we analyzed are listed as follows:

Continuous base case: the same bridge described in Section 3.3;

Case 1: Negative moment capacities are increased by +20%;

Case 2: Negative moment capacities are increased by + 40%;

Case 3: Negative moment capacities are increased by + 60%.

The Moment curvature curves for Cases 1 through 3 are compared to the base case as shown in Figure 3.17. The load deflection curves for the Base case and Cases 1 through 3 are shown in Figure 3.18 and Figure 3.19. The redundancy ratios are summarized in Table 3.7. Figure 3.20 plots the relationship between the redundancy ratios and negative bending moment capacities.

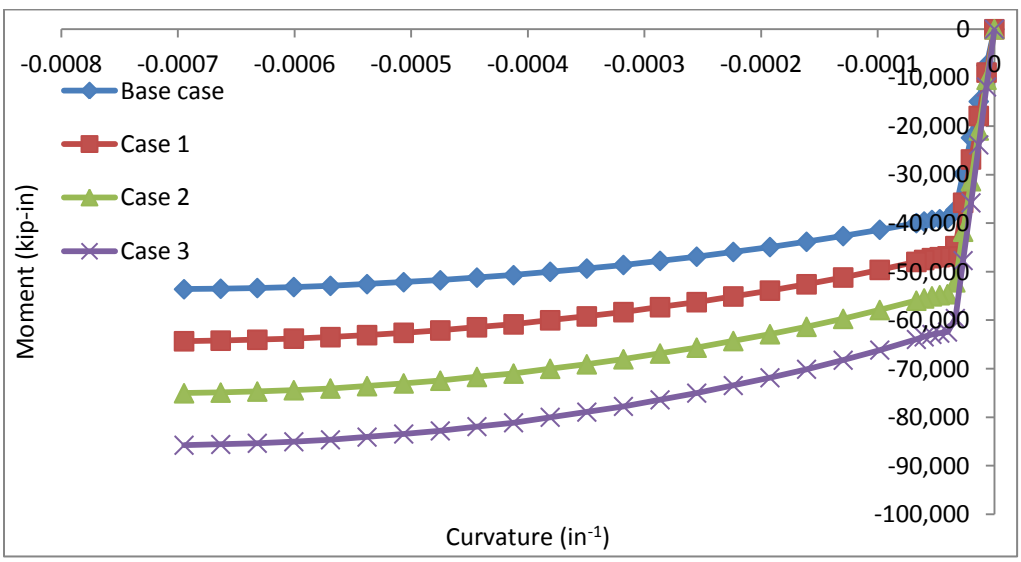


**Figure 3.17 Moment-curvature curves for different negative bending capacities**

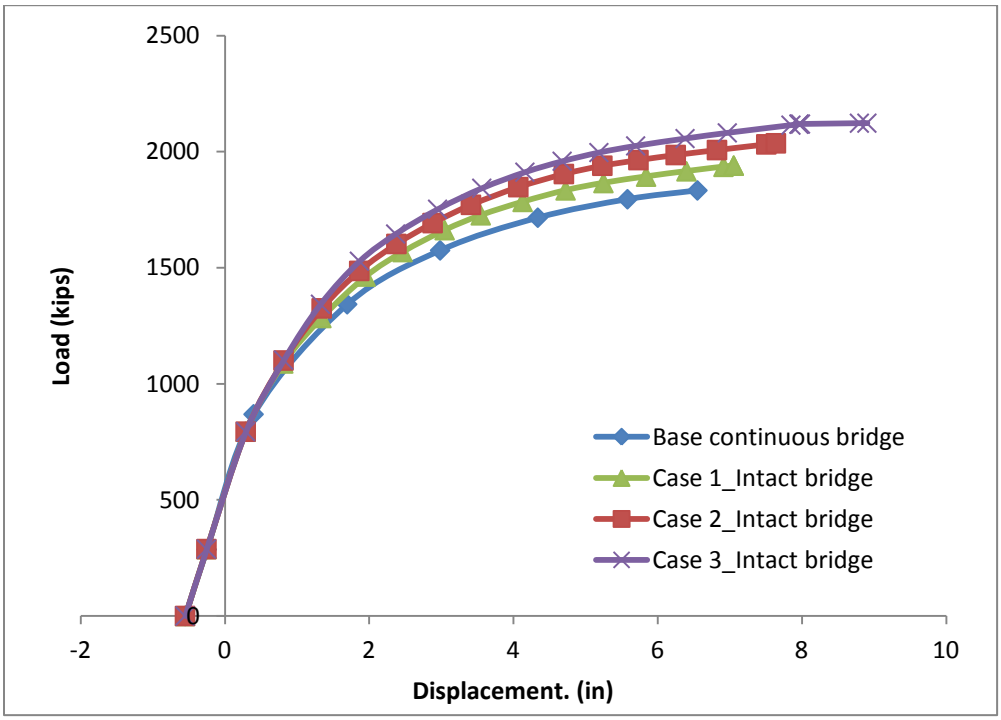


**Figure 3.18 Load deflection curves of the ultimate limit state for the continuous bridge with different negative moment capacities**

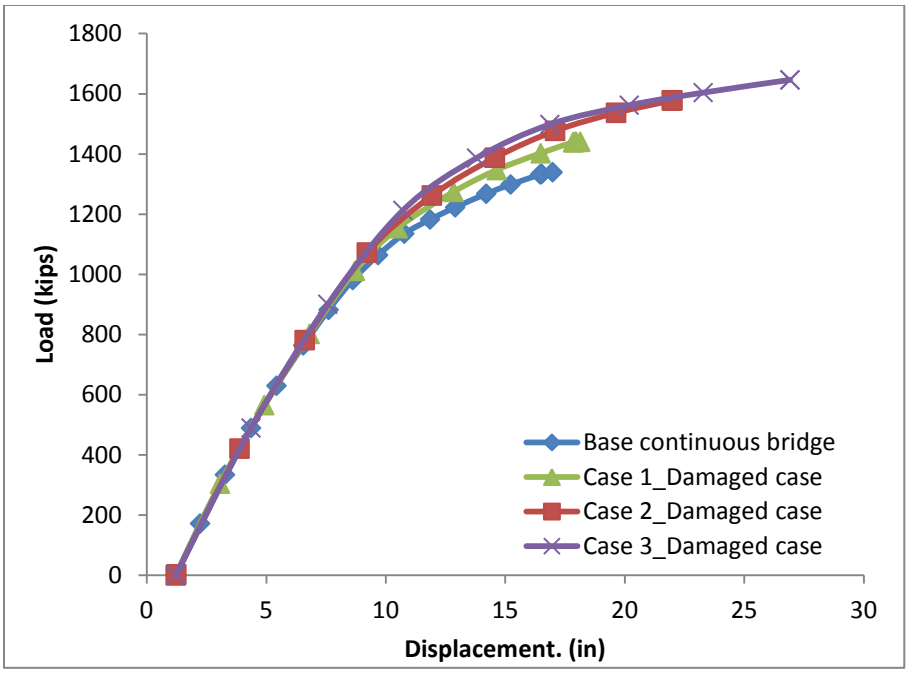


(a) The damage scenario 1

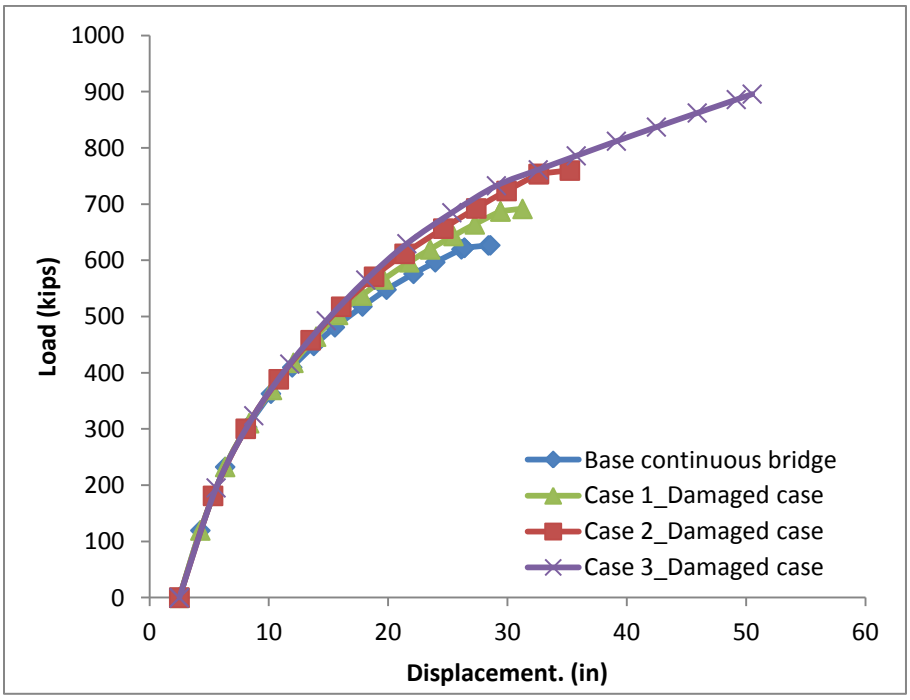


(b) The damage scenario 2

**Figure 3.19 Load deflection curves of two damaged scenarios for the continuous bridge with different negative moment capacities**

The ultimate capacities for the base continuous bridge and Cases 1 through 3 correspond to a total applied live load varying from 1,833.8 kips to respectively 1,940.6 kips and 2,037.0 kips and 2,123.6 kips. The analysis of the damaged bridge scenario 1 shows that the ultimate capacities are reached when the applied live load reaches 1,339.3 kips, 1,440.5 kips, 1,578.3 kips and 1,646.4 kips. For the damaged bridge scenario 2, the ultimate capacities are reached when the applied live load reaches 627.0 kips, 691.7 kips, 760.0 kips and 896.0 kips. The results are summarized in Table 3.7.

**Table 3.7 Summary of results for the continuous bridges with different negative bending moments**

| Cases | $R^*$ (kip-in) | $LF_1$ | $LF_u$ | $LF_d$① | $LF_d$② | $R_u$ | $R_d$① | $R_d$② |
|---|---|---|---|---|---|---|---|---|
| Base 3-span bridge | 53,600 | 23.76 | 25.47 | 18.60 | 8.71 | 1.07 | 0.78 | 0.37 |
| Case 1 | 64,320 (+20%) | 23.76 | 26.95 | 20.01 | 9.61 | 1.13 | 0.84 | 0.40 |
| Case 2 | 75,040 (+40%) | 23.76 | 28.29 | 21.92 | 10.56 | 1.19 | 0.92 | 0.44 |
| Case 3 | 85,760 (+60%) | 23.76 | 29.50 | 22.87 | 12.44 | 1.24 | 0.96 | 0.52 |

Note: * Negative bending moment capacities;

① and ② represent the damage scenario1 and 2 mentioned in Section 2.2, respectively.

From Table 3.7, we can see that the change in the redundancy ratio for the ultimate limit state, $R_u$ and the damaged scenario, $R_d$① and $R_d$② is about 16%, 23% and 40% with a maximum value of $R_u$=1.24, $R_d$①=0.96 and $R_d$②=0.52 as the negative bending moment capacity is increased by up to 60%. Figure 3.20 plots the change in the redundancy ratios as a function of the change in the negative bending capacities. From Figure 3.20, we can observe that the relationship between the redundancy ratios and negative bending moment capacities is approximately linear wit ha positive slope whereby the reudancy ratio increases as the negative bending moment capacity is increased.

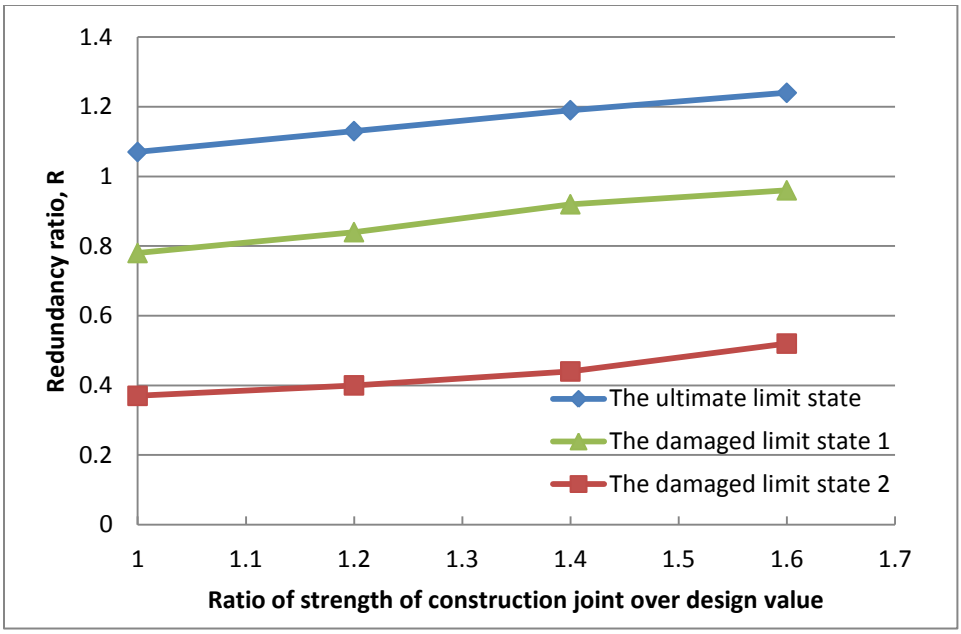


**Figure 3.20 Relationship between the redundancy ratios and negative bending capacity**

**(2) Positive bending moment capacity of middle span beams are changed**

The analysis is performed assuming that the box bridge is weaker than that of the base continuous bridge whose design is conservative having a capacity roughly about 1.8 times of what would be required. The cases we analyzed are listed as follows:

Case 1: Positive Moment capacity - 10%;

Case 2: Positive Moment capacity - 20%;

Case 2: Positive Moment capacity - 50%;

The moment curvature curves for Cases 1 through 3 are compared to the base case as shown in Figure 3.21. The load deflection curves for the Base case and Cases 1 through 3 are shown in Figure 3.22 and Figure 3.23. The redundancy ratios are summarized in Table 3.8.

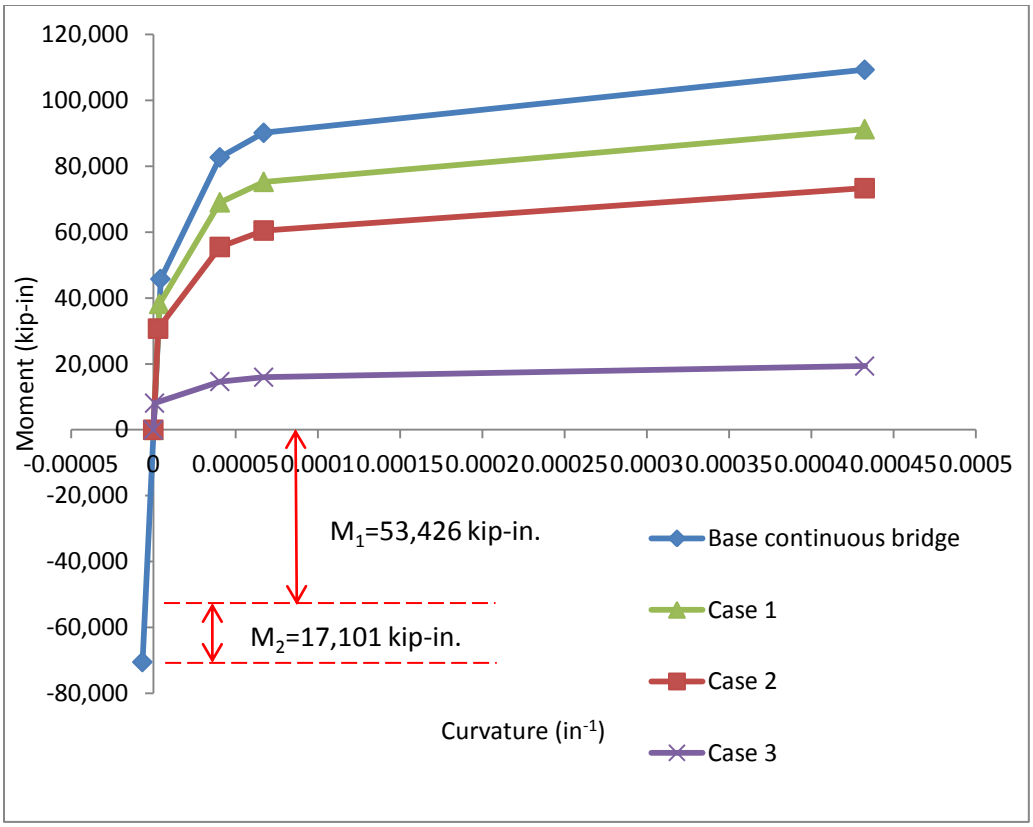


**Figure 3.21 Moment-curvature curves of longitudinal beam for different positive bending capacities**

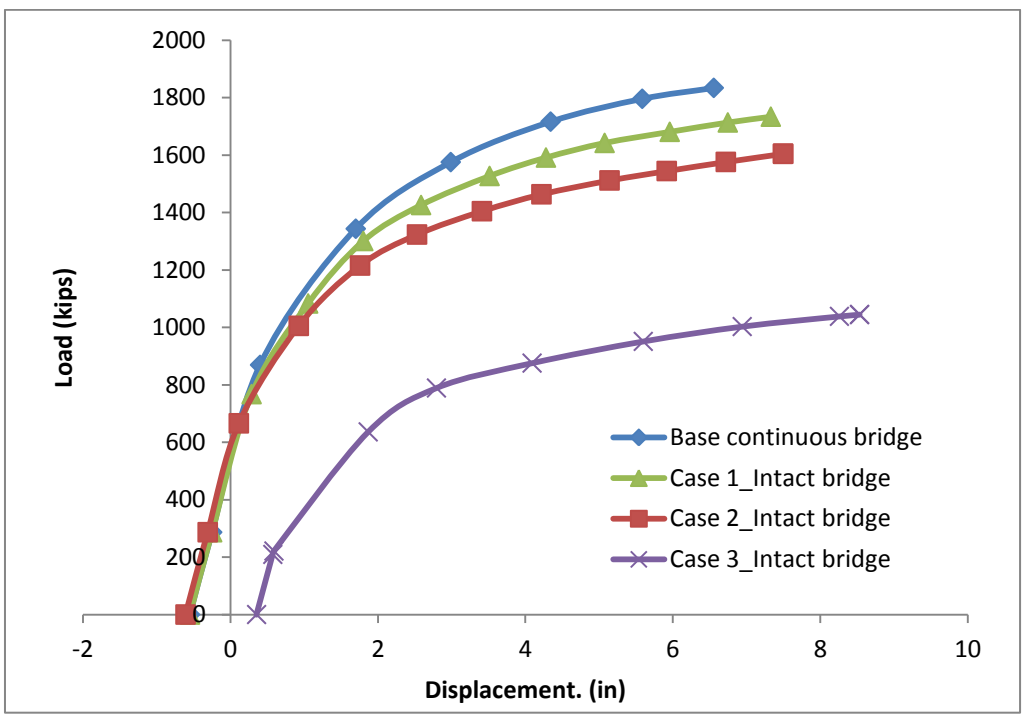


**Figure 3.22 Load deflection curves of the ultimate limit state for the continuous bridge with different positive moment capacities**

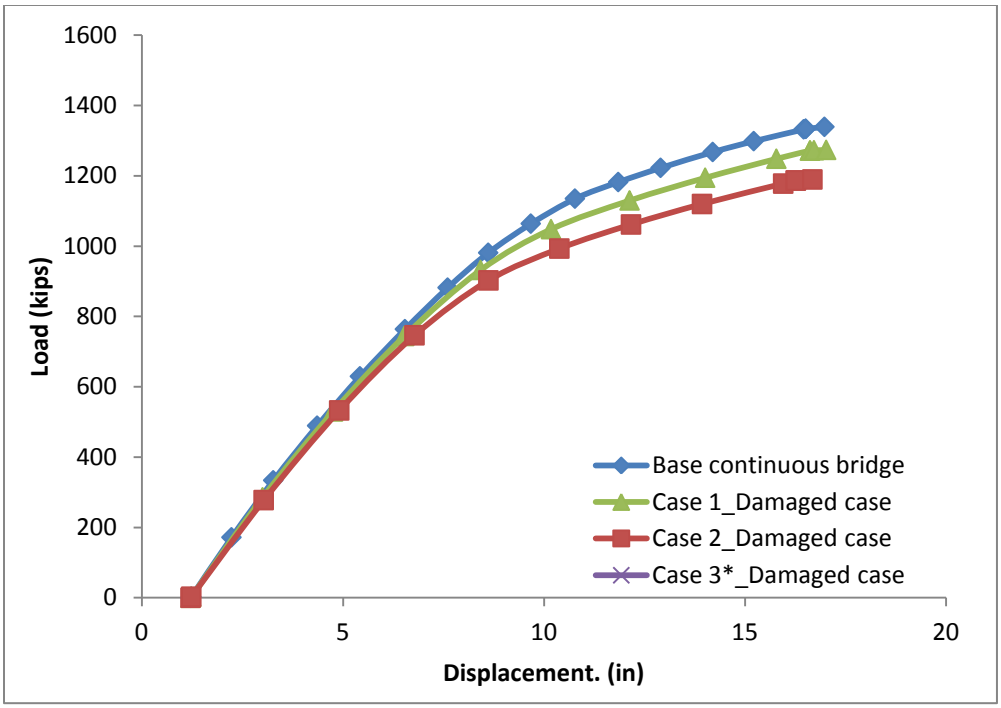


(a) The damage scenario 1

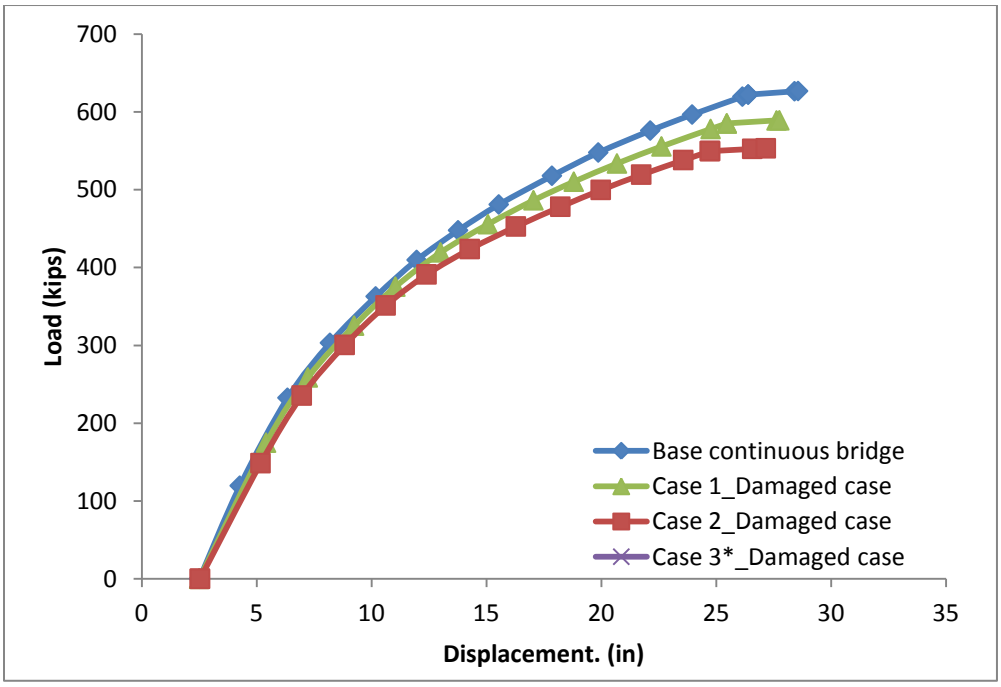


(b) The damage scenario 2

Note: * The bridge fails under the self weight for the two damaged scenarios

**Figure 3.23 Load deflection curves of damaged scenario for continuous bridge with different positive moment capacities**

The ultimate capacities for the base continuous bridge and Cases 1 through 3 correspond to a total applied live load varying from 1833.8 kips, to respectively 1,733.5 kips, 1,604.4 kips and 1,044.9 kips. The analysis of the damaged bridge scenario 1 shows that the ultimate capacities are reached when the applied live load reaches 1,339.3 kips for the base case, 1,273.8 kips, 1,189.6 kips for cases 1 and 2. For the damaged bridge scenario 2, the ultimate capacities are reached when the applied live load reaches 627.0 kips, 589.4 kips and 553.4 kips. The bridge fails under its dead load for the two damaged scenarios for Case 3.

**Table 3.8 Summary of results for the continuous bridges with different moment capacities**

| Cases | R(kip-in) | $LF_1$ | $LF_u$ | $LF_d^{①}$ | $LF_d^{②}$ | $R_u$ | $R_d^{①}$ | $R_d^{②}$ |
|---|---|---|---|---|---|---|---|---|
| Base 3-span bridge | 179,577 | 23.76 | 25.47 | 18.60 | 8.71 | 1.07 | 0.78 | 0.34 |
| Case 1 | 161,619 | 20.39 | 24.08 | 17.69 | 8.19 | 1.18 | 0.87 | 0.40 |
| Case 2 | 143,662 | 17.01 | 22.28 | 16.52 | 7.69 | 1.31 | 0.97 | 0.45 |
| Case 3 | 92,800 | 7.46 | 14.51 | --* | --* | 1.94 | --* | --* |

Note: ① and ② represent the damage scenario1 and 2 mentioned in Section 2.2, respectively.

* The bridge fails under its dead load for the two damage scenarios .

From Table 3.8, we can see that the change in the redundancy ratio for the ultimate limit state, $R_u$ and the damaged scenario, $R_d^{①}$ and $R_d^{②}$ is about 81%, 24% and 32% with a maximum value of $R_u$=1.94, $R_d^{①}$ =0.97 and $R_d^{②}$ =0.45 as the positive moment capacity of middle span beams is decreased by up to 50%. Figure 3.24 plots the redundancy ratios as a function of the change in positive moment capacity. We can observe that the relationship between the redundancy ratios is inversely related to the positive moment strength showing an increase in redundancy as the strength decreases and the change is approximately linear for small changes of up to 20% in the positive moment capacity. When the change in the positive moment capacity is 50%, the redundancy ratio for the damage condition drops to zero as the bridge fails under the effect of the dead load alone.

The redundancy ratio for the ultimate capacity deviates from the linear curve to show a larger increase in redundancy than would have been predicted with the initial slope.

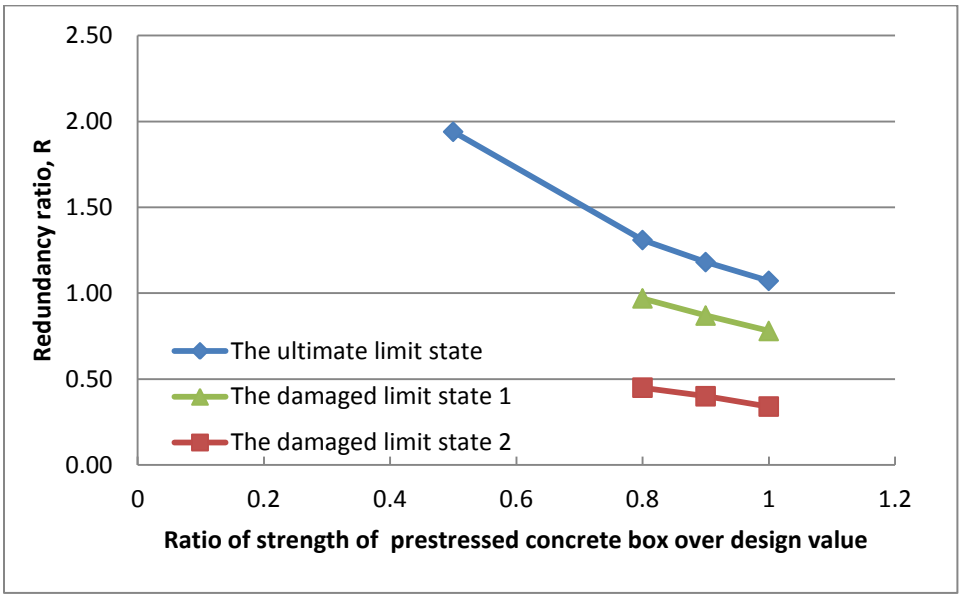


**Figure 3.24 Relationship between the redundancy ratios and positive bending capacity**

## 4. Conclusions

This report analyzed the redundancy of concrete box girder bridges under the effect of vertical loads and performed a parametric analysis to identify the primary variables that control the redundancy of such systems. From this preliminary analysis, the following observations are made:

1. The redundancy ratios of concrete box girder bridges are somewhat similar to those obtained for steel box-girder bridges as described in the previous QPR.
2. The number of bearings supports under the boxes has no effect on the redundancy ratios.
3. The analysis of two damage scenarios shows that the redundancy ratio $R_d$ decreases by about 29% if we assume that the loss in the load carrying capacity of the external web is also associated with the loss in the torsional capacity of the box as compared to the case when the torsional capacity remains the same as that of the intact box. The allowable percentage of damaged tendons in the external box should not exceed 79% in order to satisfy the redundancy criterion $R_d$=0.5 that was proposed in NCHRP 406.
4. If the bridge is designed to have continuity for live loads, it will have slightly lower redundancy ratios for both the ultimate limit state and damaged limit state than those of the simple span bridge.
5. The redundancy ratio $R_u$ for the ultimate limit state is not sensitive to changes in the member capacities or the dead load intensities for simple span bridges. However, changes in member resistances will change the redundancy ratios for the damaged limit state by a percentage on the order of about 60% of the change in member capacity.
6. Bridges that are continuous for live load will see their redundancy ratios increase when we increase the negative bending capacity or when decreasing the positive moment capacity of the middle span.

# 5. References

1. Hambly EC. (1991) Bridge Deck Behavior. London: Chapman and Hall, Ltd;

2. Hovell CG. (2007) Evaluation of Redundancy in Trapezoidal Box Girder Bridges Using Finite Element Analysis. In: The University of Texas at Austin; 2007.

3. Neuman BJ. (2009) Evaluating the redundancy of steel bridges: Full-scale destructive testing of a fracture critical twin box-girder steel bridge. In: The University of Texas at Austin; 2009.

4. Zokaie T, Osterkamp TA, Imbsen RA. (1991) Distribution of Wheel loads on Highway Bridges. NCHRP project 12-26; Transportation Research Board, The National Academies, 1991.

5. Ghosn, M., and Moses, F., (1998). *Redundancy in Highway Bridge Superstructures*. National Cooperative Highway Research Program, NCHRP Report 406, Transportation Research Board, Washington DC: National Academy Press.

6. Wright RN, Abdel-Samad SR. (1968) BEF for analysis of box girders. Journal of the Structural Division, ASCE 1968; Vol. 94, pp.1719-43.

7. Collins, M.P. and D. Mitchell (1991). *Prestressed Concrete Structures*. Prentice-Hall, Englewood Cliffs, NJ.

8. Mander, J.B., Priestly, M.J.N., “Observed Stress-Strain Behavior of Confined Concrete”, Journal of Structural Engineering, ASCE, Vol.114, No.8, August 1988, pp. 1827-1849